ORNL/TM-2001/271

OAK RIDGE
NATIONAL LABORATORY
MANAGED BY UT-BATTELLE
FOR THE DEPARTMENT OF ENERGY

EVALUATION OF SILICON NEUTRON RESONANCE PARAMETERS IN THE ENERGY RANGE THERMAL TO 1800 KEV

August 2002

Prepared by
H. Derrien, L. C. LEAL, K. H. GUBER, T. VALENTINE,
N. M. LARSON, AND T. RAUSCHER

UT-BATTELLE
ORNL-27 (4-00)

ORNL/TM-2001/271

Nuclear Science and Technology Division

EVALUATION OF SILICON NEUTRON RESONANCE PARAMETERS IN THE ENERGY RANGE THERMAL TO 1800 keV

H. Derrien, L. C. Leal, K. H. Guber, T. Valentine, N. M. Larson, and T. Rauscher*

August 2002

Prepared by
OAK RIDGE NATIONAL LABORATORY
P.O. Box 2008
Oak Ridge, Tennessee 37831-6285
managed by
UT-Battelle, LLC
for the
U.S. DEPARTMENT OF ENERGY
under contract DE-AC05-00OR22725

*Institut f. Physik, Universitad Basel, Basel, Switzerland

CONTENTS

LIST OF FIGURES

Figure **Page**

LIST OF TABLES

Table **Page**

ABSTRACT

The evaluation of the neutron cross sections of the three stable isotopes of silicon in the energy range thermal to 20 MeV was performed by Hetrick *et al*. for ENDF/B-VI (Evaluated Nuclear Data File). Resonance parameters were obtained in the energy range thermal to 1500 keV from a SAMMY analysis of the Oak Ridge National Laboratory experimental neutron transmission data. A new measurement of the capture cross section of natural silicon in the energy range 1 to 700 keV has recently been performed at the Oak Ridge Electron Linear Accelerator. Results of this measurement were used in a SAMMY re-evaluation of the resonance parameters, allowing determination of the capture width of a large number of resonances. The experimental data base is described; properties of the resonance parameters are given. For the first time the direct neutron capture component has been taken into account from the calculation by Rauscher *et al*. in the energy range from thermal to 1 MeV. Results of benchmark calculations are also given. The new evaluation is available in the ENDF/B-VI format.

I. INTRODUCTION

The last evaluation of ^{28,29,30}Si neutron induced cross sections for ENDF/B-VI was performed at ORNL by Hetrick *et al*.[1] The corresponding evaluation of the resonance parameters was based primarily on the SAMMY[2] analysis of transmission measurements of natural silicon and high enriched ^{29}Si and ^{30}Si oxide samples, performed at Oak Ridge National Laboratory (ORNL) with the Oak Ridge Electron Linear Accelerator (ORELA) neutron beam. The neutron capture widths were mainly those recommended by Mughabghab *et al*.[3] The capture cross section of natural silicon has recently been measured at ORELA by Guber *et al*.[4] in the energy range 1 to 700 keV. Reevaluation of the resonance parameters was undertaken by including the new capture cross section measurement in the experimental data base used as input to SAMMY. In the present report the experimental data base is described. The results of the new SAMMY analysis are given, and the cross sections calculated with the resonance parameters are compared to the experimental data. Properties of the resonance parameters are presented. The results were tested by performing benchmark calculations in both thermal and intermediate energy ranges.

II. THE EXPERIMENTAL DATA BASE

The following experimental data were used as input for the SAMMY analysis:

1. Neutron transmission measurement of a sample of natural silicon of thickness 0.3472 at/b in the energy range 300 to 1800 keV, performed in 1993 by Harvey *et al*.[5] at the 200-m flight path of ORELA. The neutron energy in this measurement was used as reference for the energy calibration of the other experimental data.

2. Neutron transmission measurement of a sample of natural silicon of thickness 0.0376 at/b in the energy range 5 eV to 700 keV, performed in 1976 by Larson *et al*.[6] at the 200-m flight path of ORELA. A readjustment of dE/E = 0.00075 of the energy scale was performed and a few points were added in the thermal energy range in order to calculate the total cross section at 0.0253 eV.

3. Neutron transmission measurement of a sample of thickness 0.666 at/b of natural silicon in the energy range 200 to 1800 keV, performed in 1972 by Perey *et al*.[7] at the 47-m flight path of ORELA. A readjustment of dE/E = 0.0070 of the energy scale was performed.

4. Total cross section of enriched ^{29}Si and ^{30}Si oxides from transmission measurements performed by Harvey *et al*.[8] in 1983 at the ORELA 80-m flight path. The thickness of the samples was 0.0334 at/b enriched at 95.3% of ^{29}Si and 0.0293 at/b enriched at 95.6% of ^{30}Si. These data were useful for the identification of the resonances of the corresponding isotopes. Unfortunately the statistical accuracy of the data was poor and many silicon resonances could be hidden by the oxygen resonances.

5. Capture cross section in the energy range 1 to 700 keV from measurements performed by Guber *et al*.[4] in 2000, at the 40-m ORELA flight path. A readjustment of the energy scale of $dE/E = 0.000026 + 0.00000135E^{1/2}$ was performed. A few points were added in the thermal region in order to calculate the cross section at 0.0253 eV.

6. Total cross sections in the thermal range measured in 1976 at the Cairo (Egypt) chopper by Adib *et al*.[9] at a flight path of 5.66 m with a sample of thickness 0.019 at/b, in the energy range 0.00254 eV to 6 eV.

The comparison of the average experimental effective total cross sections of Harvey, Larson, and Perey are shown in Table 1 in energy ranges where the experimental data are overlapping. In these energy ranges between resonances, where the cross section does not show any structure, the average effective cross section should be equal to the true average total cross section. The data of Harvey and of

Larson are in good agreement, but the Perey average total cross sections are about 2% larger than those of Harvey. This 2% discrepancy should correspond to a 4% error in the experimental transmission data, at the limit of the errors given by Perey. The sample used in the Perey transmission measurement had a thickness of 0.67 at/b; the transmission at the peak of the strong resonances was very small (a few percent) and the effect of the background error could be important. There is no overlapping energy region in the data of Adib measured up to 6 eV neutron energy and the data of Larson measured from 6 eV neutron energy; at 6 eV there is a discontinuity of 20% between the two measurements; the Adib data are larger. The total cross section obtained from Adib at 0.0253 eV is 2.46 b, which is 10% larger than the Mughabghab *et al*.[3] recommended value of 2.24 b. Extrapolating the data of Larson to 0.0253 eV by using the shape of the cross section calculated by the resonance parameters gives the value of 2.12 b, which is 6% smaller than the Mugaghghab value.

Table 1. Comparison of experimental effective total cross sections of natural silicon

Energy range (keV)	Average total cross section (b)[a]		
	Harvey *et al*.[5]	Larson *et al*.[6]	Perey *et al*.[7]
310–330	3.972	3.927 (-1.1%)	4.048 (2.0%)
360–380	3.507	3.523 (0.5%)	3.594 (2.5%)
390–410	3.474	3.450 (-0.7%)	3.514 (1.2%)
420–510	3.079	3.083 (0.1%)	3.124 (1.5%)
670–700	2.592	2.638 (1.8%)	2.632 (1.5%)
1050–1100	3.020		3.115 (3.1%)
1300–1390	2.702		2.782 (3.0%)
1700–1800	1.949		2.009 (3.1%)

[a]The percentage deviations are given relative to the Harvey *et al.* data.

III. *SAMMY* ANALYSIS OF THE EXPERIMENTAL DATA

The spin and parity I^{π} for the nuclei ^{28}Si, ^{29}Si, and ^{30}Si are 0^+, $1/2^+$, and 0^+, respectively. The spin and parity J^{π} of the resonances excited in the ^{29}Si, ^{30}Si and ^{31}Si compound nuclei by the neutrons of angular momentum l = 0, 1, 2 and 3 are given in Table 2. In running SAMMY, resonances are assigned to a particular spin group, each of which is characterized by spin and parity; the spin group contains the interfering resonances of the Reich-Moore formalism. Within SAMMY, it is possible to include as many neutron channels as needed; two (or more) entrance channel spins and all possible contributions of different neutron angular momenta are permitted. However, in the ENDF/B-VI Reich-Moore format, only one neutron entrance channel is allowed. One must therefore confine the SAMMY analysis to one entrance channel, in order to conform to the ENDF Reich-Moore format. For ^{28}Si and ^{30}Si, of spin $I^{\pi} = 0^+$, there is no ambiguity; the spin groups can be defined in the same way with the SAMMY rules and with ENDF/B-VI rules. But for ^{29}Si, of spin $1/2^+$, the resonances of spin and parity 1^-, 2^+, and 3^- have two neutron entrance channels. A physically sound calculation of the cross sections could be performed by using two components of the neutron widths, and the transformation into the ENDF/B-VI format could be

possible by adding in a single channel the contribution of the two neutron channels of the SAMMY calculations. However, the shape of the calculated cross sections could be quite different in the case of strong interference effects. To ensure the consistency between the SAMMY calculations and the ENDF calculations, the resonance groups should be defined according to the same *l*, *s*, and J values. In this configuration, 13 groups of resonances, with $l \leq 3$, can be considered for ^{29}Si (see Table 2). There are two groups of 1^- resonances, two groups of 2^+ resonances, and two groups of 3^- resonances. Only one neutron channel is used in each group, but the two groups of same spin are not interfering, which could bring difficulties in fitting the experimental data in case of strong interference effects. In this case, the change into the ENDF/B-VI format is possible because a recent modification[10] of the format allows adding the flag + or - to the spin of the resonance (+ for the channel spin s = I+1/2 and - for the channel spin s = I - 1/2). In the present evaluation, the resonance parameter file contains the seven spin groups of ^{28}Si resonance of angular momenta $l \leq 3$; but only the angular momenta $l \leq 2$ were considered for ^{29}Si and ^{30}Si (ten groups for ^{29}Si, compatible with the ENDF/B-VI format, and five groups for ^{30}Si). The ^{16}O resonance parameters, which were needed for the analysis of the SiO_2 transmission data, were taken from the recent evaluation by Sayer *et al.*[11]

Table 2. The resonance spins of ^{28}Si, ^{29}Si, and ^{30}Si

	l	$s = I \pm 1/2$	J^π
^{28}Si (0^+)	0	1/2	$1/2^+$
and	1	1/2	$1/2^-$ $3/2^-$
^{30}Si (0^+)	2	1/2	$3/2^+$ $5/2^+$
	3	1/2	$5/2^-$ $7/2^-$
^{29}Si ($½^+$)	0	0	0^+
	1	0	1^-
	1	1	0^- 1^- 2^-
	2	0	2^+
	2	1	1^+ 2^+ 3^+
	3	0	3^-
	3	1	2^- 3^- 4^-

The prior values of the resonance parameters were those obtained in the previous evaluation by Hetrick *et al.*[1] for ENDF/B-VI. The radiative capture widths were obtained primarily from the BNL recommended data.[3] In the present evaluation, Guber *et al.*[4] experimental capture data were analyzed in the energy range from 1 to 700 keV. Self-shielding and multiple scattering effects were taken into account in the SAMMY calculations. At the beginning of the analysis, the fit of the capture data was performed separately for each individual resonance appearing in the experimental data. Some resonances, with very small neutron width values, were not seen in the transmission data; these resonances are at the energies 16.672, 31.751, 70.840, 86.993, 147.681, 298.800, 369.79 and, 399.621 keV; they were assigned to ^{28}Si, except for the resonance at 369.79 keV, which was assigned to ^{29}Si.

The sequential SAMMY analysis of the natural silicon experimental transmission and capture data was performed by allowing a search on the normalization and background correction parameters, using the associated SAMMY-SAMAMR sequences for updating the resonance covariance file between the analysis of each individual experiment. The final SAMMY analysis was an Implicit Data Covariance type (IDC) sequential calculation, using in the IDC input files the systematic error information obtained in the SAMMY-SAMMAR analysis, allowing realistic calculation of the covariance values of the input experimental data. The resonance parameters obtained from the analysis are given in Tables 3–5. The covariance file is too large to be included in the present report and can be obtained upon request from the authors. Correction for the neutron sensitivity of the ORELA capture detector was not performed for the

capture widths. An upper limit for the correction could be obtained by using the following relation, due to Koehler *et al.*[12] : $C = 2.4\ 10^{-4}\ E_r^{-0.8}\ \Gamma_n$, where the resonance energy E_r is given in keV and the correction is in the same unit as the neutron width Γ_n. The correction is negligible compared with the experimental errors, with the exception of the ^{28}Si resonances at 55.7, 182.5, and 565.7 keV, where the correction is 3.7, 2.9, and 1.2%, respectively, for the upper limit.

Compared with the previous evaluation, the following improvements were obtained in the present work:

1. At 67.7 and 354.5 keV, it was not possible to simultaneously fit the capture data and the transmission data with a single resonance having a realistic value of the capture width. It is likely that these resonances are doublets at energies 67.75 and 67.79 keV, and 354.49 and 354.65 keV, respectively. The two resonances in each doublet were attributed to the ^{28}Si isotope since no resonance at these energies could be identified in the SiO_2 transmission data.

2. Better fits were obtained by modifying the spins of some weak ^{28}Si resonances. These resonances have values of neutron widths of the same order of magnitude as the width of the resolution function. It is then possible to choose without ambiguity the value of the statistical factor g from the shape of the resonance. Examples are given in Figs. 1–3. Actually, the small resonances in the transmission data were examined individually, allowing determination of the best value of the neutron widths concurrently with the best spin determination.

3. The number and the parameters of the ^{28}Si external fictitious resonances were modified: two negative energy fictitious resonances instead of five, and three resonances in the energy range above 1800 keV instead of seven. Better fits to the transmission data were obtained, particularly in the high-energy region.

Table 3. The Reich-Moore resonance parameters of ^{28}Si

Energy (keV)	l	J	Capture width (eV)	Neutron width (eV)
-4635.300	0	0.5	0.2000E+01	0.5437E+07
-28.801	0	0.5	0.6950E+01	0.2450E+03
16.762	1	1.5	0.1409E+01	0.3383E-03
31.751	2	2.5	0.3080E+00	0.1319E-01
55.735	0	0.5	0.1698E+00	0.6613E+03
67.746	3	3.5	0.5709E+00	0.2653E+00
67.790	3	2.5	0.1773E+00	0.1426E+01
70.841	2	2.5	0.5495E+00	0.1107E-01
86.994	1	1.5	0.1960E+00	0.8148E+00
147.681	1	1.5	0.4353E+00	0.4015E-01
182.545	0	0.5	0.4405E+01	0.3502E+05
298.800	2	2.5	0.3976E+00	0.1438E+01
354.495	2	2.5	0.2590E+00	0.8501E+01
354.648	2	1.5	0.1536E+00	0.2292E+02
399.621	1	1.5	0.7710E+00	0.9360E+00
532.664	2	2.5	0.5046E+00	0.5473E+03
565.666	1	1.5	0.1451E+01	0.1089E+05
587.164	2	1.5	0.8716E+00	0.2478E+03
590.296	0	0.5	0.3174E+00	0.5399E+03
602.439	1	0.5	0.4229E+01	0.1311E+03
714.043	1	1.5	0.1409E+01	0.1242E+01

Table 3. (Cont.)

Energy (keV)	l	J	Capture width (eV)	Neutron width (eV)
771.712	2	2.5	0.4360E+00	0.6937E+02
812.482	1	1.5	0.3290E+01	0.2967E+05
845.239	2	1.5	0.6800E+00	0.4379E+03
872.301	2	2.5	0.4420E+00	0.4638E+02
910.048	1	1.5	0.3840E+00	0.3547E+04
961.896	1	0.5	0.5440E+01	0.7916E+05
1017.783	2	2.5	0.4360E+00	0.9798E+02
1042.876	2	2.5	0.3570E+00	0.9872E+03
1085.169	0	0.5	0.1634E+01	0.8695E+02
1149.004	3	3.5	0.3830E+00	0.1573E+02
1162.681	0	0.5	0.1292E+01	0.2851E+04
1200.464	1	0.5	0.2585E+01	0.1533E+05
1201.347	0	0.5	0.1634E+01	0.3480E+04
1257.159	0	0.5	0.1634E+01	0.1719E+05
1264.471	2	2.5	0.7310E+00	0.9347E+03
1380.077	2	2.5	0.4360E+00	0.6275E+02
1408.396	1	1.5	0.9180E+00	0.5286E+04
1479.982	2	1.5	0.4360E+00	0.3748E+04
1482.395	1	0.5	0.1409E+01	0.8861E+00
1512.193	3	3.5	0.3830E+00	0.9769E+02
1528.795	2	1.5	0.4360E+00	0.2908E+04
1580.748	2	1.5	0.4360E+00	0.1161E+04
1587.500	2	2.5	0.4360E+00	0.7482E+02
1598.496	1	0.5	0.1409E+01	0.6625E+04
1595.440	2	1.5	0.4360E+00	0.6194E+04
1639.882	2	2.5	0.4360E+00	0.1510E+05
1651.183	2	2.5	0.4360E+00	0.2284E+05
1658.563	1	0.5	0.1409E+01	0.1538E+04
1664.961	2	1.5	0.4360E+00	0.2807E+03
1784.855	2	1.5	0.4360E+00	0.1307E+03
1805.653	1	1.5	0.1409E+01	0.1180E+04
1909.667	2	2.5	0.1000E+01	0.6215E+05
1915.435	1	1.5	0.2500E+01	0.1427E+06
2458.765	0	0.5	0.3600E+01	0.3696E+06

Table 4. The Reich-Moore resonance parameters of ^{29}Si

Energy (keV)	l	J	Capture width (eV)	Neutron width (eV)
-2041.700	0	0.0	0.1539E+03	0.2061E+07
-859.350	0	0.0	0.9998E+01	0.3147E+05
-431.280	0	0.0	0.6006E+01	0.4018E+03
15.294	1	1.0	0.1265E+01	0.5012E+01
38.834	1	2.0	0.2241E+01	0.8776E+02
159.877	1	1.0	0.2688E+01	0.1202E+04
184.594	1	1.0	0.2645E+01	0.1369E+03
336.936	1	2.0	0.7039E+00	0.1208E+04
374.032	1	0.0	0.4623E+01	0.1072E+06
384.222	0	1.0	0.5173E+01	0.8910E+04
389.162	1	1.0	0.5805E+01	0.2415E+02
480.664	1	0.0	0.6305E+01	0.2077E+05
553.201	1	2.0	0.2834E+01	0.1299E+04
565.000	1	1.0	0.4193E+01	0.6656E+05
600.718	1	0.0	0.2000E+01	0.3886E+05
620.353	2	3.0	0.1594E+01	0.8432E+03
650.301	1	2.0	0.7414E+00	0.1109E+04
652.522	1	1.0	0.7590E+01	0.3067E+05
715.065	1	1.0	0.3000E+00	0.9786E+03
872.484	1	1.0	0.3000E+00	0.1600E+05
955.891	1	2.0	0.3000E+00	0.9829E+03
1098.426	2	1.0	0.3000E+01	0.5779E+02
1113.808	1	1.0	0.3000E+00	0.6764E+05
1120.280	1	2.0	0.3000E+00	0.4882E+04
1183.602	0	1.0	0.3000E+01	0.8296E+04
1192.268	1	1.0	0.3000E+00	0.3751E+03
1207.630	1	2.0	0.3000E+00	0.2957E+05
1240.000	1	1.0	0.3000E+00	0.9924E+04
1388.859	2	1.0	0.3000E+01	0.4271E+04
1769.073	0	0.0	0.3000E+01	0.3214E+02
2248.487	0	0.0	0.3000E+01	0.1693E+03

Table 5. The Reich-Moore resonance parameters of ^{30}Si

Energy (keV)	l	J	Capture width (eV)	Neutron width (eV)
-1147.400	0	0.5	0.1708E+02	0.2682E+06
-161.550	0	0.5	0.6500E+00	0.2640E+04
4.981	1	1.5	0.2287E+00	0.1334E+01
15.145	1	1.5	0.1024E+00	0.1135E+01
183.489	0	0.5	0.8367E+01	0.1014E+05
190.226	1	1.5	0.7695E+00	0.1013E+02
235.205	2	1.5	0.9042E+00	0.1154E+03
302.807	1	1.5	0.3625E+00	0.2743E+03
413.389	1	1.5	0.5644E+00	0.1581E+04
645.600	2	1.5	0.3547E+00	0.4009E+03
705.625	2	2.5	0.8000E+00	0.3231E+03
745.454	1	1.5	0.3700E+00	0.1467E+05
796.946	1	1.5	0.6000E+00	0.4693E+03
807.380	1	1.5	0.6000E+00	0.2743E+03
810.797	1	1.5	0.6000E+00	0.4193E+03
844.675	1	1.5	0.3700E+00	0.6615E+04
879.801	2	2.5	0.8000E+00	0.2899E+03
979.821	1	1.5	0.6000E+00	0.5918E+03
1182.176	0	0.5	0.6000E+01	0.5912E+04
1217.821	2	1.5	0.8000E+00	0.4589E+04
1274.872	1	1.5	0.6000E+00	0.2226E+04
1302.033	2	1.5	0.8000E+00	0.3048E+03
1310.775	1	1.5	0.3700E+00	0.3397E+03
1333.910	1	1.5	0.6000E+00	0.4624E+04
1356.025	1	1.5	0.3700E+00	0.1227E+05
1383.598	1	1.5	0.6000E+00	0.2534E+05
1400.981	2	1.5	0.8000E+00	0.1008E+04
1412.108	1	1.5	0.3700E+00	0.6686E+03
1586.007	0	0.5	0.6000E+01	0.2364E+05
2583.250	0	0.5	0.6000E+01	0.9208E+05

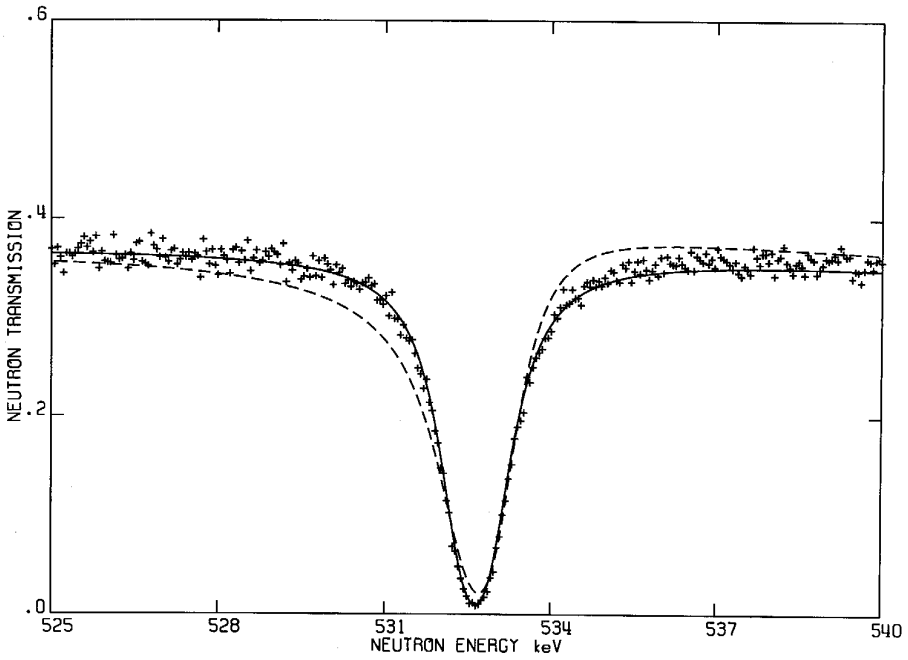

Fig. 1. Neutron transmission in the resonance at 532.7 keV. The crosses represent Harvey *et al.*[5] experimental data. The solid and dashed lines are the SAMMY fit of the data for angular momentum and spin l = 2, J = 2.5, and l = 1, J = 1.5, respectively.

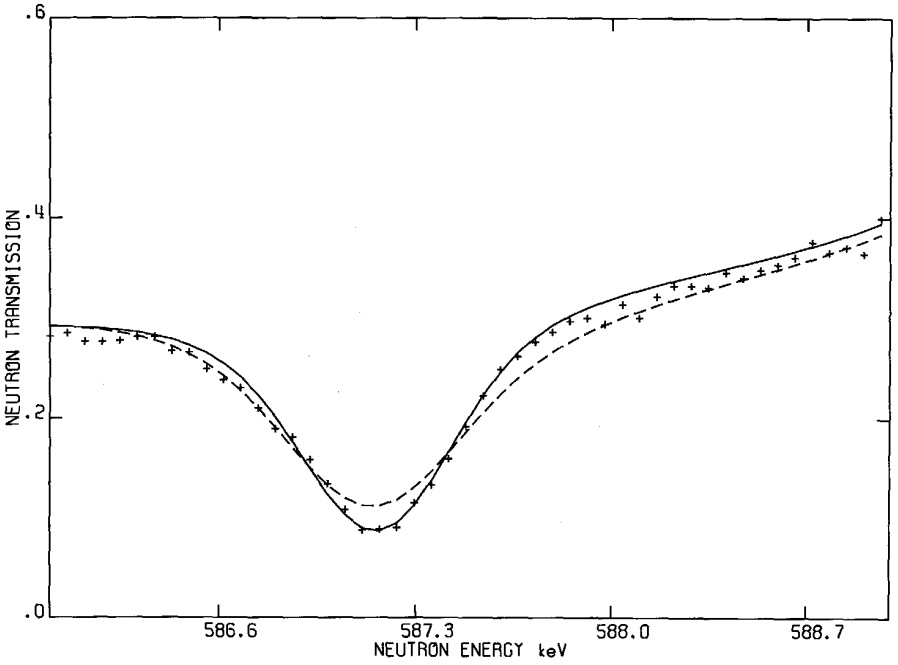

Fig. 2. Neutron transmission in the resonance at 587.2 keV. The crosses represent Harvey *et al.*[5] experimental data. The solid and dashed lines are the SAMMY fit of the data for angular momentum and spin l = 2, J = 1.5, and l = 1, J = 0.5, respectively.

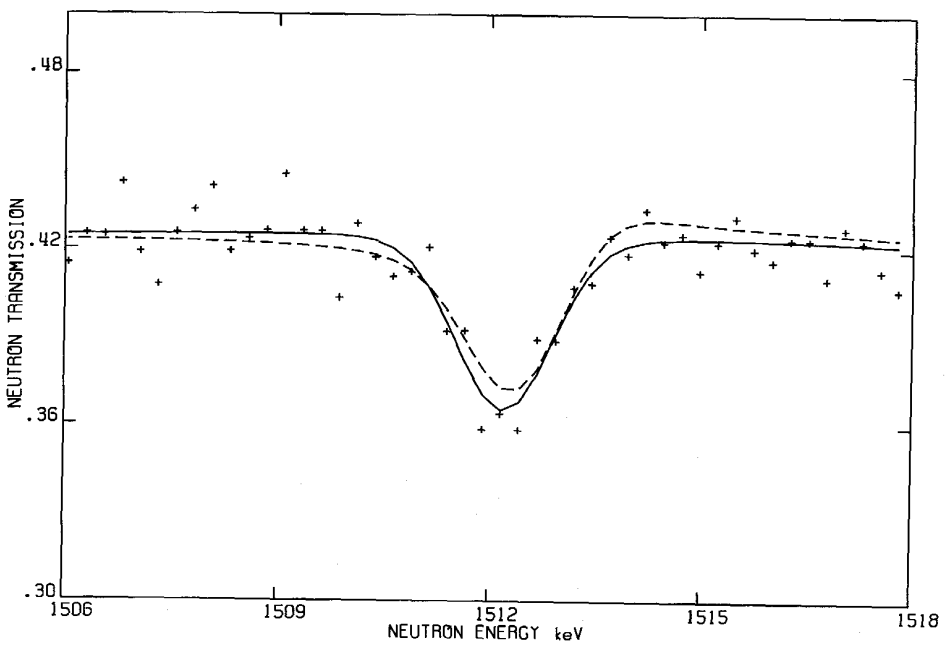

Fig. 3. Neutron transmission in the resonance at 1512.3 keV. The crosses represent Harvey *et al.*[5] experimental data. The solid and dashed lines are the SAMMY fit of the data for angular momentum and spin l = 3, J = 3.5, and l = 2, J = 2.5, respectively.

IV. THE RESONANCE PARAMETERS

IV.1. The Neutron Strength Function of ^{28}Si

The fit of the data was obtained with 49 resonances of ^{28}Si in the energy range from thermal to 1800 keV, with the spin distribution given in Table 6. The neutron strength functions corresponding to this distribution are $S_0 = (0.79 \pm 0.45) \times 10^{-4}$, $S_1 = (1.03 \pm 0.40) \times 10^{-4}$ and $S_2 = (1.37 \pm 0.40) \times 10^{-4}$, for the angular momenta $l = 0$, $l = 1$, and $l = 2$, respectively. The errors are the sampling errors obtained from the relative value $(2/N)^{1/2}$, N being the number of resonances in each sample. The values of S_1 and S_2 could be questioned since the spin assignment of the resonances was made in order to obtain the best fit to the experimental transmission data, and is probably not the unique solution. However, they do not contradict the values that are found for other nuclei in the corresponding mass region, as is shown in Fig. 4 and Fig. 5, derived from Mughabghab *et al.*[3]

The last column in Table 6 shows the expected number of resonances for each J value obtained by applying the 2J + 1 dependance of the level density to the number of observed s-wave resonances. For l = 1 and $l = 2$, the number of assigned spins is smaller than the expected number, but is comparable. It is likely that resonances with small values of the neutron widths are missing in the experimental data; there are only 4 resonances in the $l = 3$ resonance groups compared with the expected 49 resonances. Actually, most of the $l = 3$ resonances are missing in the experimental data due to the small values of the penetration factor in the energy range of analysis.

Table 6. The resonance spin repartition of ^{28}Si

Number of observed resonances	Angular momentum (l)	Spin (J)	Number of expected resonances
7	0	0.5	7
6	1	0.5	7
9	1	1.5	14
9	2	1.5	14
14	2	2.5	21
1	3	2.5	21
3	3	3.5	28

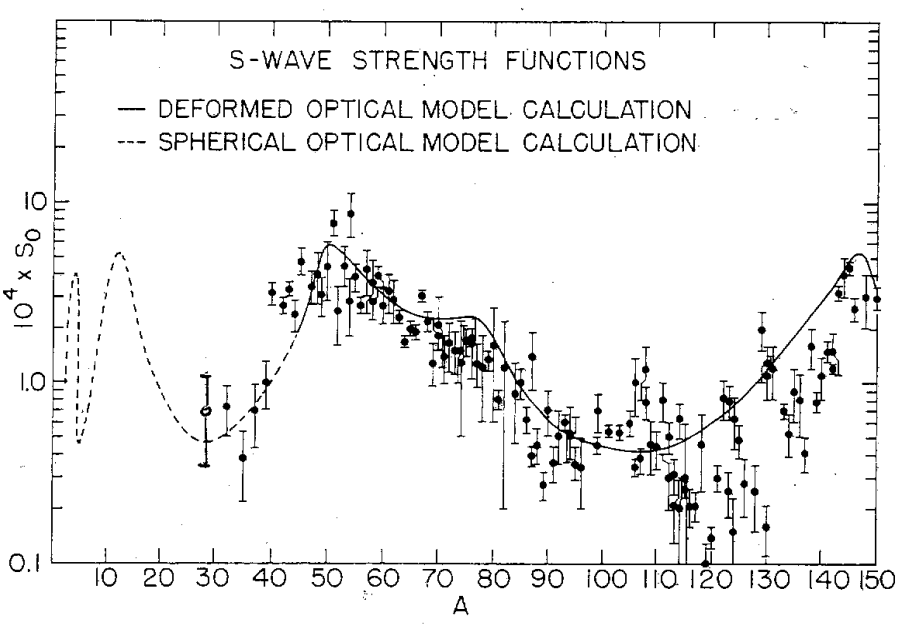

Fig. 4. Variation of the s-wave neutron strength function with the mass of the nucleus. The circle shows the value obtained for ^{28}Si in the present evaluation. This figure has been adapted from Mughabghab *et al*. (Ref. 3).

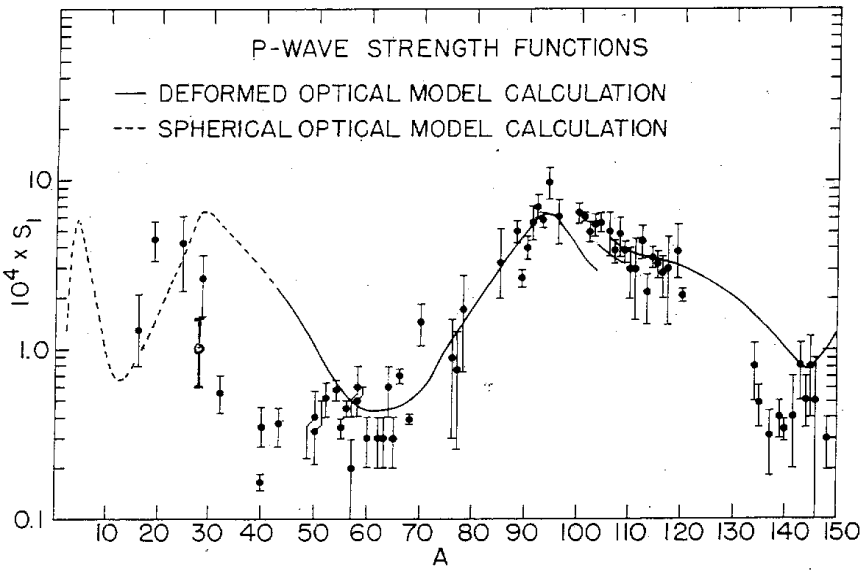

Fig. 5. Variation of the p-wave neutron strength function with the mass of the nucleus. The circle shows the value obtained for ^{28}Si in the present evaluation. This figure has been adapted from Mughabghab *et al*. (Ref. 3).

The values of the s-wave, p-wave, and d-wave neutron strength functions were obtained by using the following relation:

$$S_l = [1 / (2l + 1)\Delta E]\Sigma g\Gamma_n^l$$

where Γ^l_n is the reduced neutron width of a resonance of angular momentum *l*. The energy interval ΔE containing the resonances of the corresponding sample was taken as the difference between the energy of the last resonance and the energy of the first resonance of the sample plus one average spacing. The reduced neutron widths were obtained by the usual relations:

s-wave $\Gamma^0_n = \Gamma_n / E^{1/2}$
p-wave $\Gamma^1_n = (\Gamma_n / E^{1/2}) (1 + P)$
d-wave $\Gamma^2_n = (\Gamma_n / E^{1/2}) (1 + 3P + 9P^2)$
with $P = 1 / k^2a^2$ and $a = 1.35 A^{1/3}$

where a is the nuclear radius and A the atomic mass.

IV.2. The Radiative Capture Parameters of ^{28}Si

The capture widths and the capture areas of the ^{28}Si resonances are given in Table 7 in the energy range up to 700 eV. The capture areas are compared with the values recommended by Mughabghab *et al*. The values obtained in the present work are smaller. The most striking discrepancy occurs for the resonance at 55.7 keV, where the value of 1.5 eV is given by Mubghabghab *et al*. and the value of 0.172 eV is obtained in the present evaluation. In the energy range above 700 keV, the capture widths recommended by Mughabghab *et al*., which were mainly based on the experimental data of Boldeman *et al*.,[13] are on average larger than in the low-energy range. Some particularly large values of 9.7, 16, and 7.8 eV are found for the resonances at 816, 964, and 1204 eV, respectively. The average capture widths obtained in the present evaluation from the analysis of the Guber *et al*. experimental data, in the energy range up to 700 eV, are 1.634 eV for the s-wave resonances (from three resonances), 1.409 eV for the p-wave resonances (from five resonances), and 0.550 eV for the d-wave resonances (from seven resonances). Each of these average capture widths is much smaller than the average value of 3.6 eV for the combined s, p and d resonances from the Mughabghab evaluation. The average value of the resonant

component of the capture cross section in the energy range 700 to 1800 keV is 0.484 mb when calculated by using the Mughabghab capture widths and only 0.171 mb by using the Mubhabghab values normalized to values consistent with Guber average values; the latter solution was taken in the final version of the present evaluation.

IV.3. The Resonance Parameters of ^{29}Si and ^{30}Si

An attempt was made to obtain the resonance parameters of ^{29}Si and ^{30}Si by analyzing the two SiO_2 transmission data sets with samples enriched to 95.3% of ^{29}Si and 95.6% of ^{30}Si, respectively. The experimental data, shown in Figs. 6 and 7, are not sufficiently accurate (poor resolution and poor statistical accuracy) to allow identification of all the resonances and a good evaluation of the neutron widths. Moreover, the strong resonances of oxygen at 434 and 1000 keV impede the analysis of a large part of the data. It is recommended that new accurate transmission measurements be made of the SiO_2 samples, with compensation for the oxygen contribution.

Table 7. The ^{28}Si resonance parameters in the energy range up to 700 keV

Resonance energy (keV)	l	J	g	Neutron width (eV)	Capture width (eV)	gΓnΓγ/Γ eV	
						This work	Mughabghab[3]
16.8	1	1.5	2	0.0003	4.330 ± 0.600	0.0008	
31.8	2	2.5	3	0.013	0.309 ± 0.030	0.038	0.048 ± 0.005
55.7	0	0.5	1	661.14 ± 2.13	0.172 ± 0.005	0.172	1.500 ± 0.020
67.7	2	3.5	4	0.27	0.587 ± 0.032		
67.8	2	2.5	3	1.43	0.179 ± 0.053		
70.8	2	2.5	3	0.011	0.550	0.033	0.038 ± 0.004
87.0	1	1.5	2	0.81	0.198 ± 0.004	0.319	
147.7	1	1.5	2	0.04	0.433 ± 0.043	0.074	
182.5	0	0.5	1	35020.00 ± 35.0	4.405 ± 0.063	4.413	5.600 ± 2.200
298.8	2	2.5	3	1.44	0.398 ± 0.011	0.941	1.160 ± 0.130
354.5	2	2.5	3	8.50 ± 0.70	0.258 ± 0.013	0.752	1.400 ± 0.150
354.7	2	1.5	2	22.92 ± 0.96	0.154 ± 0.014	0.313	
399.6	1	1.5	2	0.94	0.771 ± 0.038	0.850	1.310 ± 0.040
532.7	2	2.5	3	547.29 ± 1.76	0.505 ± 0.017	1.513	1.900 ± 0.300
565.7	1	1.5	2	10894.00 ± 15.7	1.451 ± 0.057	2.835	5.800 ± 0.900
587.2	2	1.5	2	247.82 ± 2.91	0.872 ± 0.030	1.730	2.800 ± 0.400
590.3	0	0.5	1	539.86 ± 5.38	0.317 ± 0.025	0.318	
602.4	1	0.5	1	131.07 ± 3.46	4.229 ± 0.093	4.090	6.800 ± 1.000

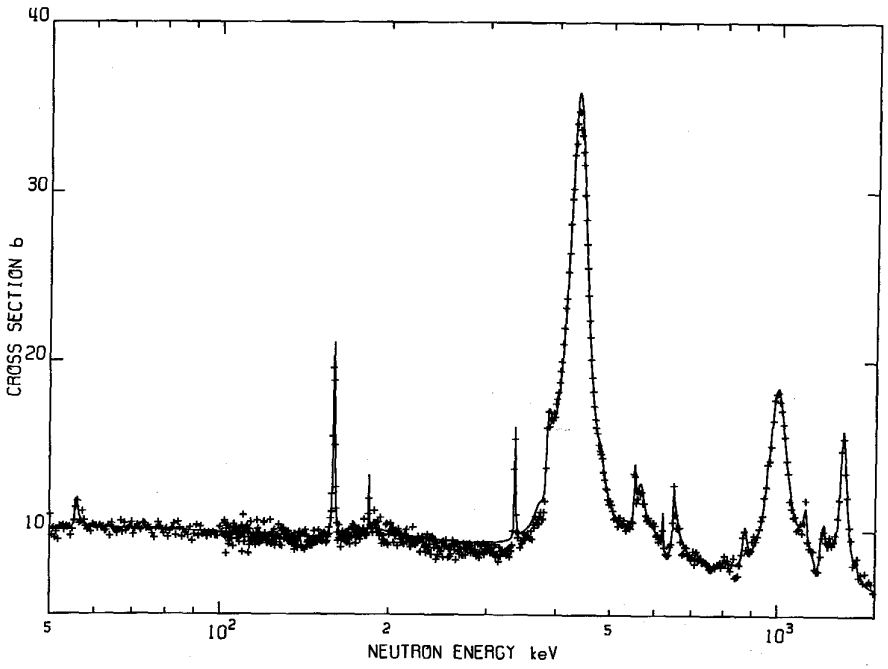

Fig. 6. The SiO_2 total cross section obtained from transmission measurement of a sample containing 0.0334 at/b of ^{29}Si with an enrichment of 95.3%. The crosses represent the experimental data of Harvey *et al*.[8] averaged by 10. The solid line represents the cross section calculated by the resonance parameters. The two strong resonances are the oxygen resonances at 433.9 and 999.7 keV.

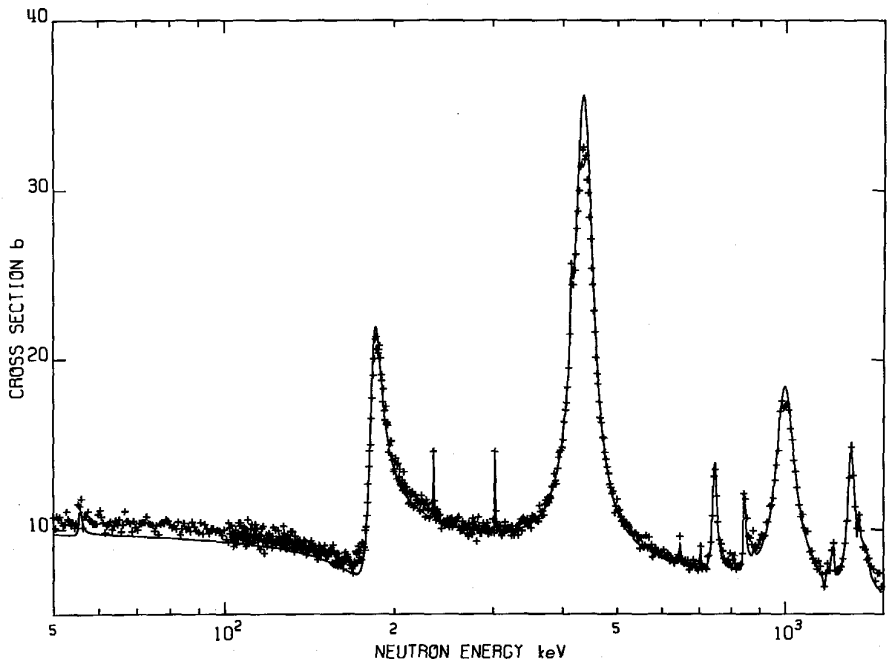

Fig. 7. The SiO_2 total cross section obtained from transmission measurement of a sample containing 0.0293 at/b of ^{30}Si with an enrichment of 95.6%. The crosses represent the experimental data of Harvey *et al*.[8] averaged by 10. The solid line represents the cross section calculated by the resonance parameters. The two strong resonances are the oxygen resonances at 433.9 and 999.7 keV.

However, the analysis of the Guber *et al*. capture data allowed the accurate evaluation of the capture area of 5 p-wave resonances of ^{29}Si at the energies 15.29, 38.83, 159.88, 184.59, and 389.16 keV, and of 3 p-waves resonances of ^{30}Si at the energies 49.81, 15.14, and 190.23 keV. The average values of the capture widths of these resonances are 2.93 and 0.37 eV, respectively, for ^{29}Si and ^{30}Si.

V. THE CALCULATED CROSS SECTIONS

V.1. General View

The neutron transmissions calculated with the resonance parameters are compared with the experimental values of Larson *et al*. and of Harvey *et al*. in Figs. 8-13. The calculated capture cross sections, including the experimental effects, are compared with the experimental values of Guber *et al*. in Figs. 14-22. The calculated average cross sections, compared to the experimental values, are given in Table 8. The calculated effective total cross section for the experimental conditions of Harvey *et al*. is 0.5% smaller than that of Larson *et al*. due to different sample effects in the transmission measurements. The calculated average capture cross section (effective cross section taking into account the experimental effects) is 11% lower than the experimental value of Guber *et al*. due to a remaining experimental background or to uncalculated contribution of direct capture.

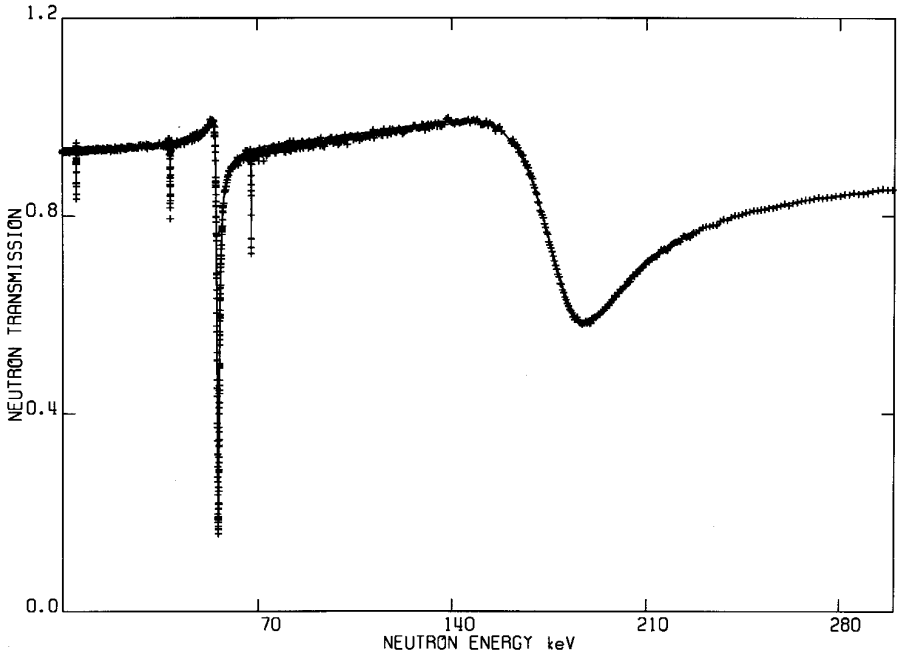

Fig. 8. Natural silicon neutron transmission in the energy range 6–300 keV. The crosses represent the experimental data of Larson *et al*.[6] The solid line represents the transmission calculated from the resonance parameters.

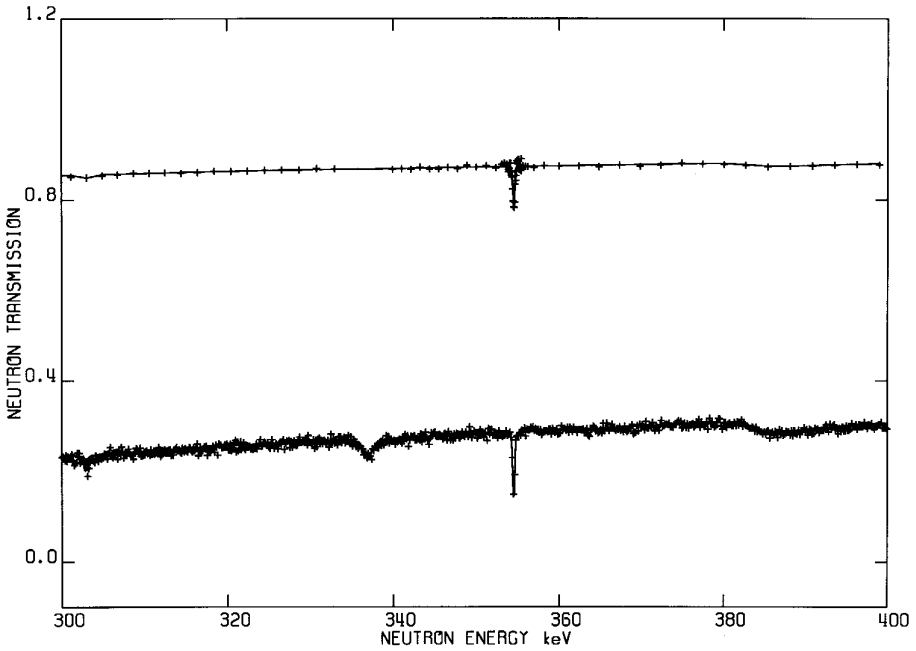

Fig. 9. Natural silicon neutron transmission in the energy range 300–400 keV. The crosses represent the experimental data of Larson *et al.*[6] (upper curves) and of Harvey *et al.*[5] (lower curves). The solid lines represent the transmission calculated from the resonance parameters.

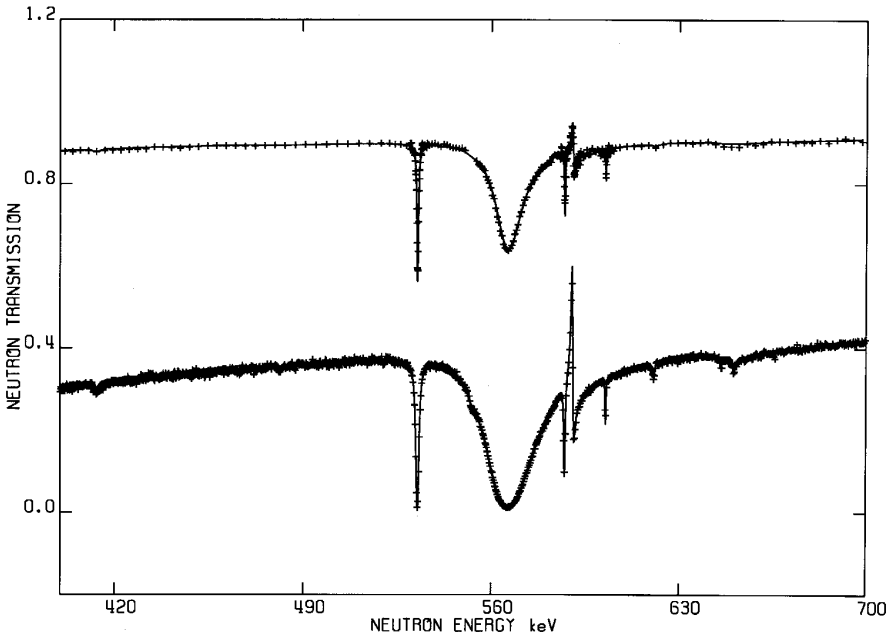

Fig. 10. Natural silicon neutron transmission in the energy range 400–700 keV. The crosses represent the experimental data of Larson *et al.*[6] (upper curves) and of Harvey *et al.*[5] (lower curves). The solid lines represent the transmission calculated from the resonance parameters.

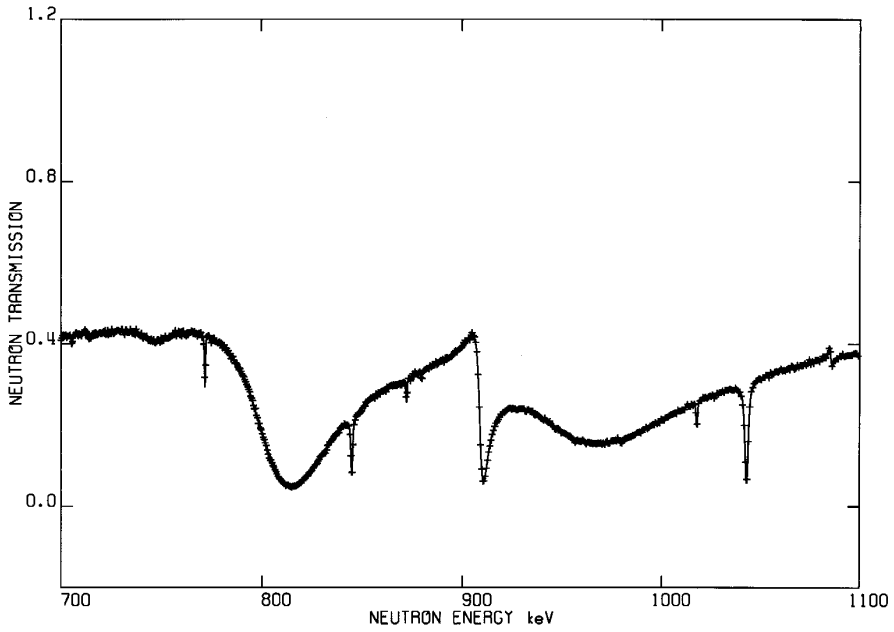

Fig. 11. Natural silicon neutron transmission in the energy range 700–1100 keV. The crosses represent the experimental data of Harvey *et al*.[5] The solid lines represent the transmission calculated from the resonance parameters.

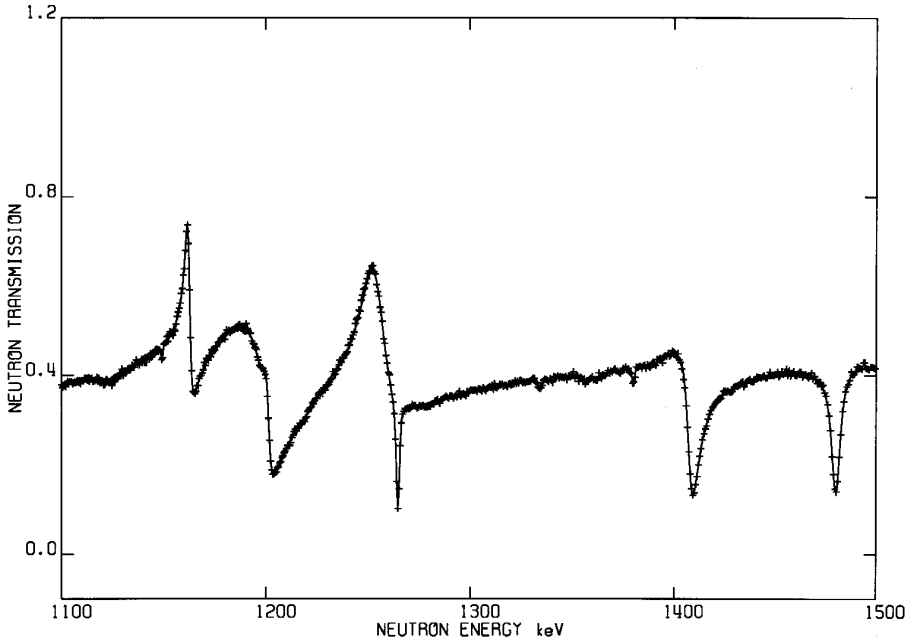

Fig. 12. Natural silicon neutron transmission in the energy range 1100–1500 keV. The crosses represent the experimental data of Harvey *et al*.[5] The solid lines represent the transmission calculated from the resonance parameters.

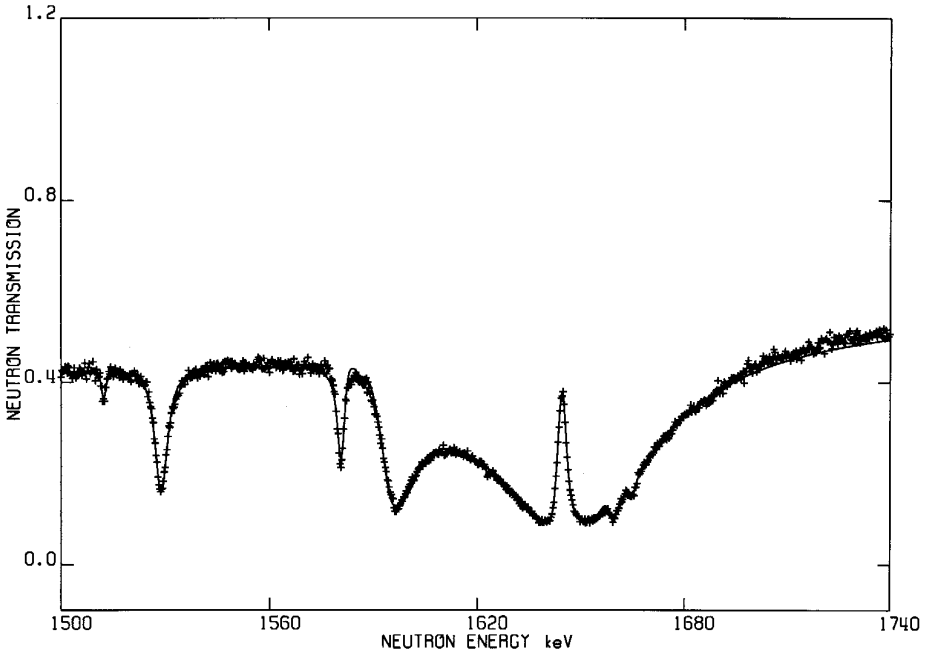

Fig. 13. Natural silicon neutron transmission in the energy range 1500–1750 keV. The crosses represent the experimental data of Harvey *et al.*[5] The solid lines represent the transmission calculated from the resonance parameters.

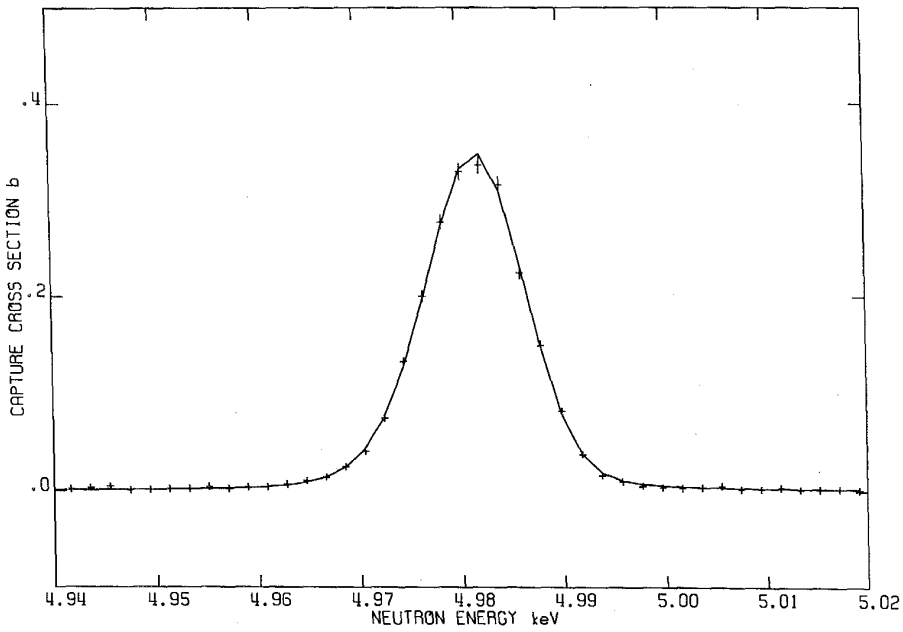

Fig. 14. Effective capture cross section of the resonance at 4.98 keV of ^{30}Si. The crosses represent the experimental data of Guber *et al.*[4] The solid line represents the data calculated with the resonance parameters, taking into account experimental effects.

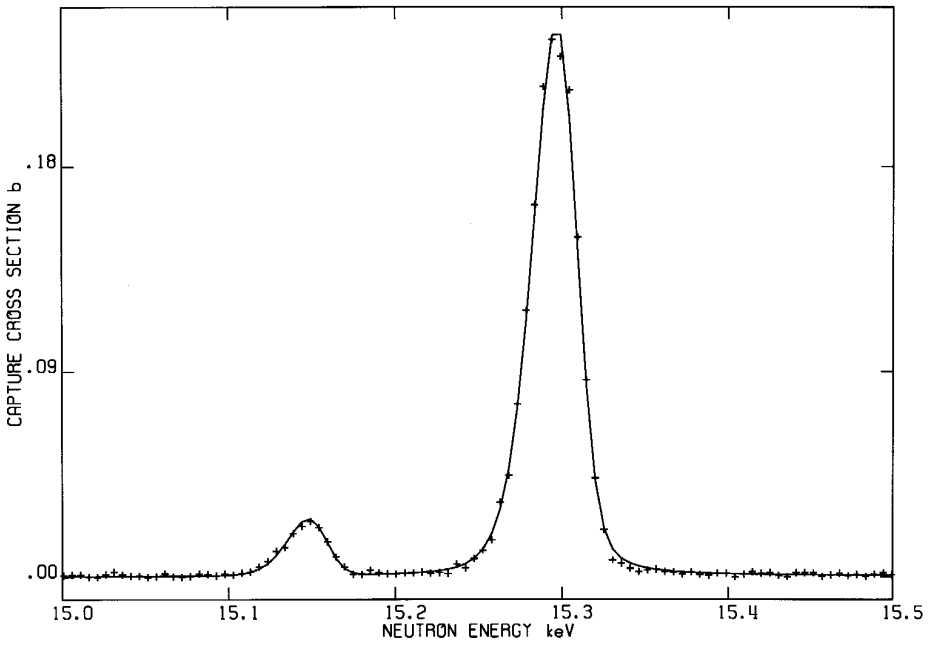

Fig. 15. Effective capture cross section of the resonance at 15.14 keV of ^{30}Si and 15.29 keV of ^{29}Si. The crosses represent the experimental data of Guber *et al.*[4] The solid line represents the data calculated with the resonance parameters, taking into account experimental effects.

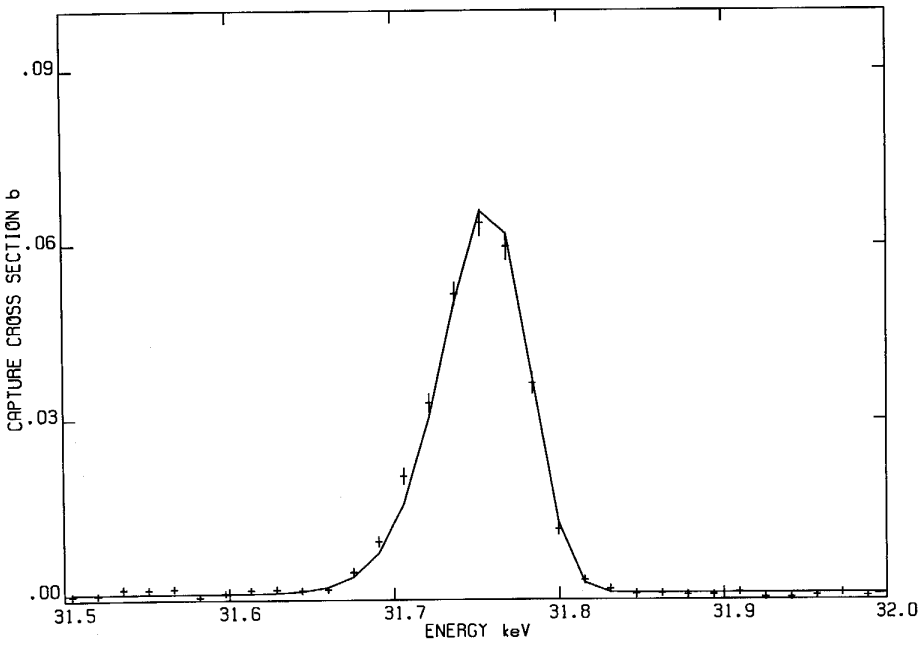

Fig. 16. Effective capture cross section of the resonance at 31.75 keV of ^{28}Si. The crosses represent the experimental data of Guber *et al.*[4] The solid line represents the data calculated with the resonance parameters, taking into account the experimental effects.

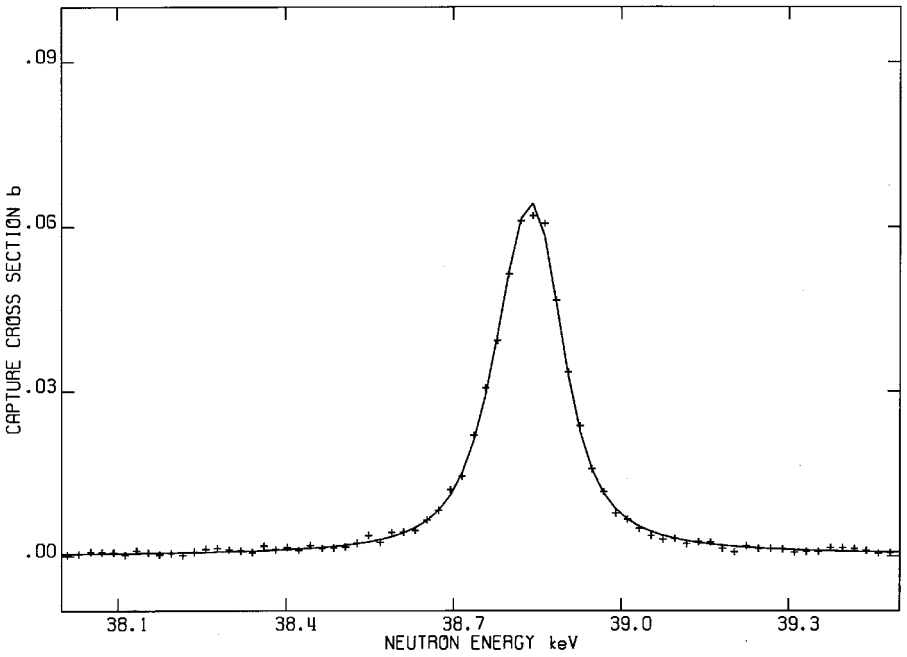

Fig. 17. Effective capture cross section of the resonance at 38.83 keV of ^{29}Si. The crosses represent the experimental data of Guber *et al.*[4] The solid line represents the data calculated with the resonance parameters, taking into account the experimental effects.

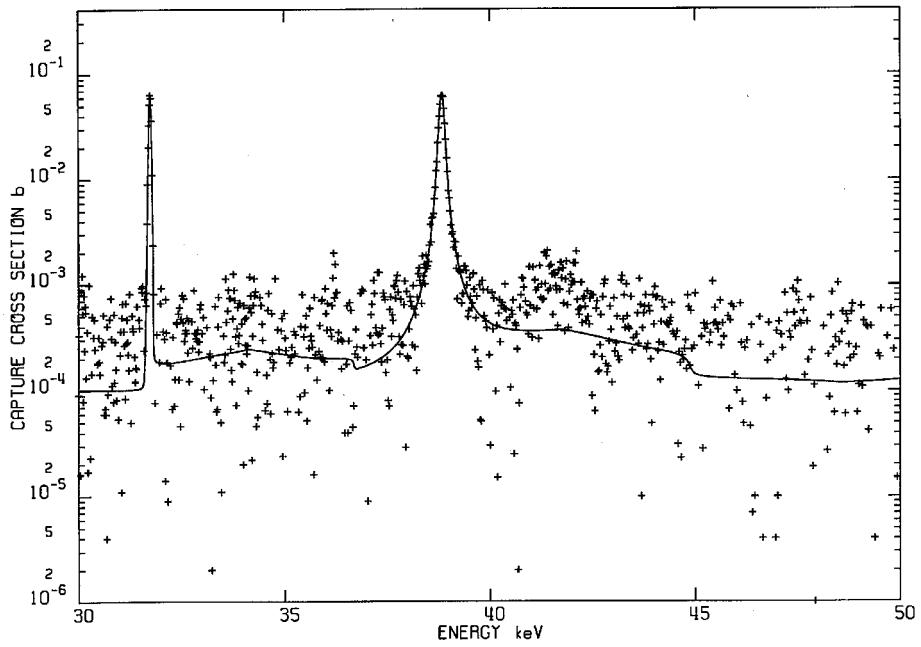

Fig. 18. Effective capture cross section of natural silicon in the energy range 30–50 keV. The crosses represent the experimental data of Guber *et al.*[4] The solid line represents the data calculated with the resonance parameters, taking into account the experimental effects. The structures seen between the resonances in the calculated effective cross section are due to the multiple scattering in the sample.

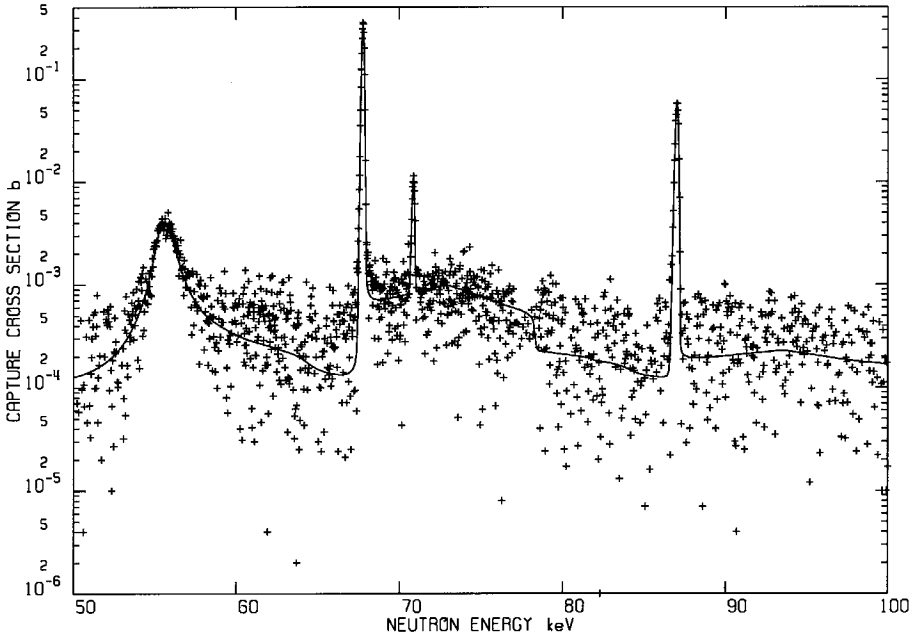

Fig. 19. Effective capture cross section of natural silicon in the energy range 50–100 keV. The crosses represent the experimental data of Guber *et al*.[4] The solid line represents the data calculated with the resonance parameters, taking into account the experimental effects. The structures seen between the resonances in the calculated effective cross section are due to the multiple scattering in the sample.

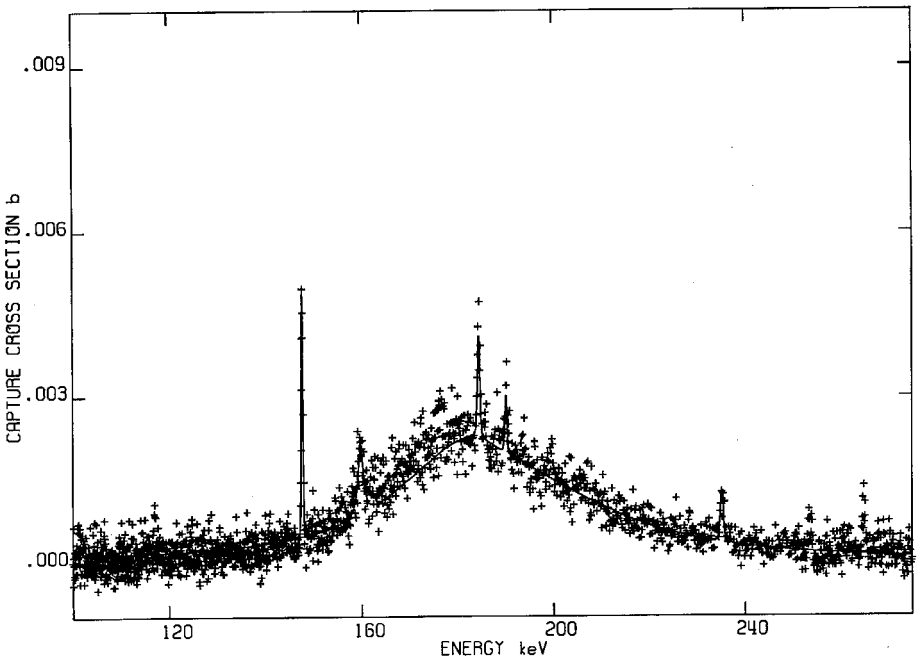

Fig. 20. Effective capture cross section of natural silicon in the energy range 100–270 keV. The crosses represent the experimental data of Guber *et al*.[3] The solid line represents the data calculated with the resonance parameters, taking into account the experimental effects.

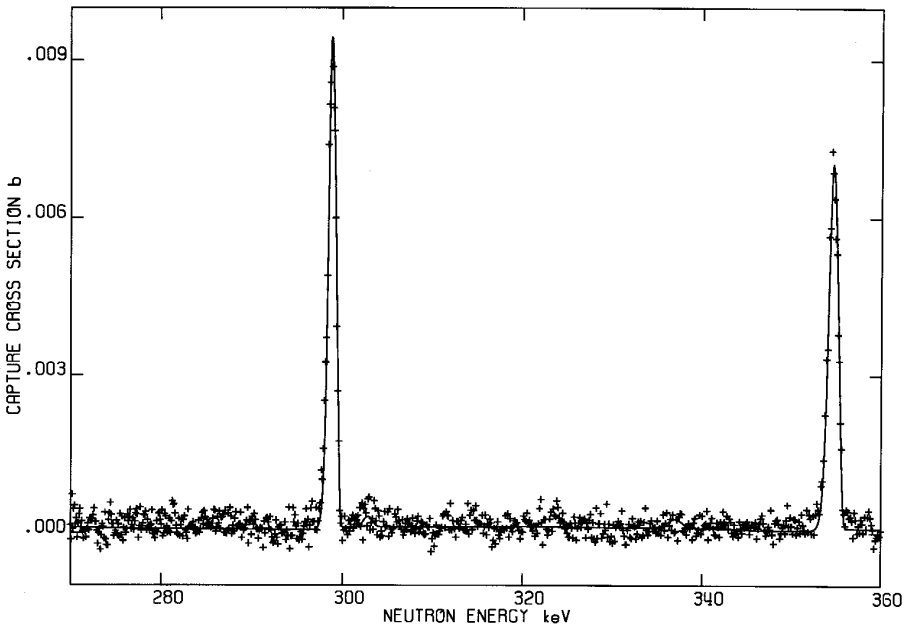

Fig. 21. Effective capture cross section of natural silicon in the energy range 270–360 keV. The crosses represent the experimental data of Guber *et al*.[4] The solid line represents the data calculated with the resonance parameters, taking into account the experimental effects.

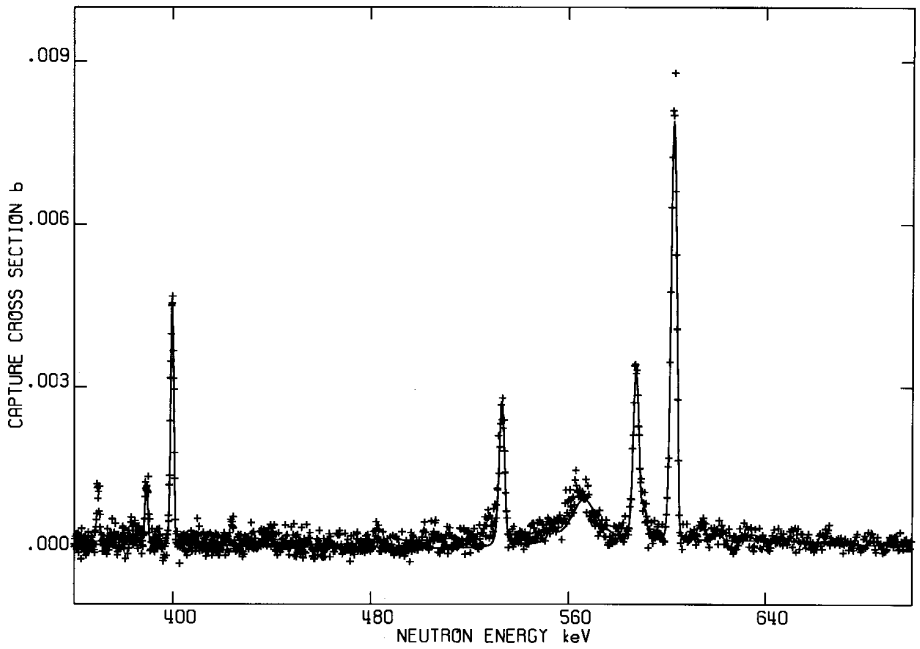

Fig. 22. Effective capture cross section of natural silicon in the energy range 360–700 keV. The crosses represent the experimental data of Guber *et al*.[4] The solid line represents the data calculated with the resonance parameters, taking into account the experimental effects.

Table 8. The average cross sections: comparison of the experimental data and the values calculated with the resonance parameters

Energy Range keV	Effective total cross section (b)				Capture cross section (mb)	
	Larson *et al*.[6]		Harvey *et al*.[5]		Guber *et al*.[4]	
	Exp.	Calc.	Exp.	Calc.	Exp.	Calc.
1.–301.	4.156	4.084 (-1.7%)				
301.–690.	3.568	3.531 (-1.0%)	3.562	3.515 (-1.3%)		
690.–1790.			3.302	3.302 (-0.0%)		
10.–690.					0.636	0.572 (-11%)

V.2. The Capture Cross Sections

In the SAMMY fit of the experimental capture data, an additional background was used in order to reproduce the measured cross section between the resonances. This additional background was meant to compensate for errors in the evaluation of the experimental background and for the direct capture component, which is not calculated by the Reich-Moore formalism. The amount of the additional background varied from 2.5 mb at 3 to 0.15 mb at 700 keV. The direct capture component was recently calculated by T. Rauscher *et al*.[14] using the TEDCA[15] code, including the E1, M1, and E2 transitions. The resulting cross sections were parametrized into s-, p-, and d-wave contributions in a lower and upper limit given by the following relations due to T. Rauscher *et al*.:

^{28}Si $\sigma_{low} = 0.7(3.050 \times 10^{-4}\ E^{-1/2} + 1.303 \times 10^{-5}\ E^{1/2} + 4.462 \times 10^{-10}\ E^{3/2})$

$\sigma_{high} = 1.3(3.448 \times 10^{-4}\ E^{-1/2} + 2.445 \times 10^{-5}\ E^{1/2} + 4.639 \times 10^{-10}\ E^{3/2})$

^{29}Si $\sigma_{low} = 0.7(2.644 \times 10^{-4}\ E^{-1/2} + 4.429 \times 10^{-5}\ E^{1/2} + 1.576 \times 10^{-10}\ E^{3/2})$

$\sigma_{high} = 1.3(3.098 \times 10^{-4}\ E^{-1/2} + 1.489 \times 10^{-4}\ E^{1/2} + 1.644 \times 10^{-10}\ E^{3/2})$

^{30}Si $\sigma_{low} = 0.7(3.172 \times 10^{-4}\ E^{-1/2} + 2.429 \times 10^{-5}\ E^{1/2} + 5.531 \times 10^{-10}\ E^{3/2})$

$\sigma_{high} = 1.3(3.479 \times 10^{-4}\ E^{-1/2} + 6.480 \times 10^{-5}\ E^{1/2} + 5.680 \times 10^{-10}\ E^{3/2})$

The variations of the calculated values versus energy are displayed in Fig. 23.

The direct capture of the natural silicon calculated from these relations is (0.235 ± 0.094) mb at 3 keV and (0.700 ± 0.412) mb at 700 keV. Due to the uncertainty of the calculated direct capture cross section and the difficulties of evaluating the experimental background in the capture cross section measurement, the values of the average total capture cross section are quite uncertain in the energy range above several keV.

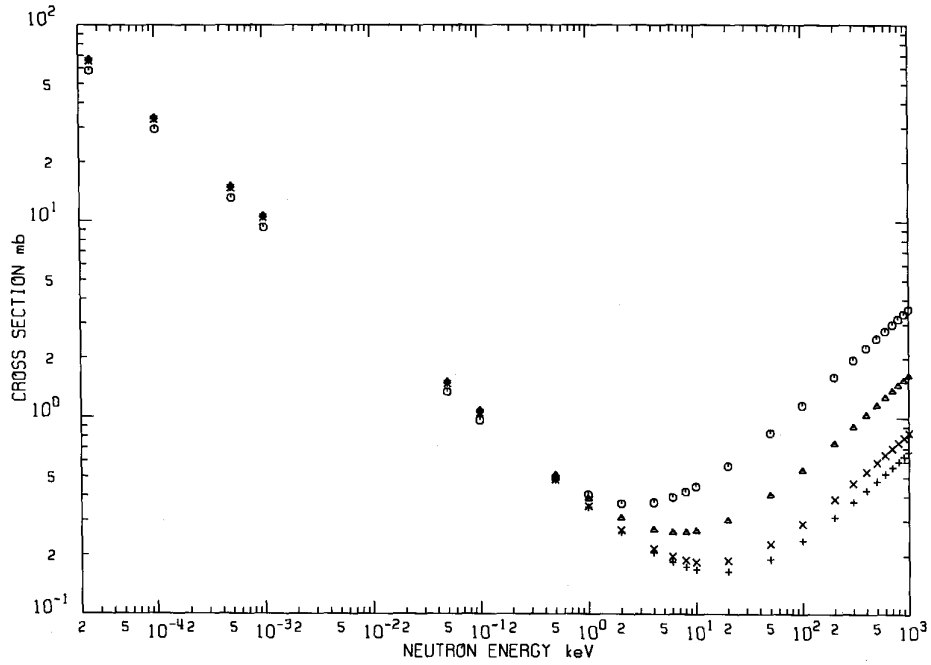

Fig. 23. Direct neutron capture cross section as calculated by Rauscher *et al.*[14] Symbols used: + = ^{28}Si, o = ^{29}Si, Δ = ^{30}Si, and x = natural silicon.

The calculated direct capture cross section at 0.0253 eV is (65.8 ± 23.3) mb, (58.4 ± 21.6) mb, (67.0 ± 22.9) mb and (65.5 ± 23.2) mb, respectively, for ^{28}Si, ^{29}Si, ^{30}Si and natural silicon. The cross sections at 0.0253 eV calculated from the resonance parameters with the contribution of the direct capture are given in Table 9. The values of the capture cross section of the three isotopes were obtained close to the values of Raman *et al.*[16] by adjusting the parameters of the negative energy resonances, with a resonant component of 103.15, 60.60, and 41.16 mb for ^{28}Si, ^{29}Si, and ^{30}Si, respectively. The values recommended by Mughabghab *et al.*,[3] those obtained by Islam *et al.*,[17] and those obtained by Kennett and Prestwich[18] are also displayed in Table 9.

At 1700 keV, near the boundary of the resolved resonance energy range, the direct capture components calculated by Rauscher *et al.* relations are (0.88 ± 0.48), (4.65 ± 3.36), (2.13 ± 1.40), and (1.10 ± 0.64) mb for ^{28}Si, ^{29}Si, ^{30}Si and ^{nat}Si, respectively. These values are much larger than the average values of the resonant components which are 0.094, 0.011, 0.018, and 0.088 mb, respectively, in the energy range 1600 to 1800 keV. On the other hand, the ENDF/B-VI values, calculated by Hetrick *et al.* with the code TNG,[19] are 0.55 mb at 1750 keV for ^{28}Si, and 1.20 mb at 1500 keV for ^{30}Si. The TNG calculation did not include the direct component, but the cross sections were normalized on measured values at 14 MeV. Matching the resolved resonance range and the high energy range is possible, as the direct component should decrease above the threshold of the inelastic scattering (1780 keV for ^{28}Si and 2235 keV for ^{29}Si). For ^{30}Si, the normalization of the TNG calculated values were not possible since there was no experimental data available in the high-energy range. The unresolved energy range starts at 1300 keV; except for the peak of 1 mb at 1390 keV (resonance identified in SiO_2 transmission data), the capture cross section calculated by TNG is smaller than 0.01 mb, which is not consistent with the calculated direct capture of 4 mb at 1300 keV. It is unlikely that this large difference could be due only to the opening of the inelastic channel at 1273 keV.

Table 9. Total and capture neutron cross sections at 0.0253 eV

	Total (b)		Capture (mb)				
	Present	Mughabghab[3]	Present	Mughabghab[3]	Kennett[18]	Islam[17]	Raman[16]
^{28}Si	2.099	2.199	168.9	177.	171 ± 3	207 ± 4	169 ± 4
^{29}Si	2.887	2.889	119.0	101.	122 ± 4	120 ± 3	119 ± 3
^{30}Si	2.599	2.597	108.2	107.	103 ± 4	107 ± 2	108 ± 3
^{nat}Si	2.150	2.244	164.7	171.			

The calculated ^{nat}Si average capture cross sections in six energy intervals in the neutron energy range up to 1750 keV are given in Table 10. Taking into account the direct capture component, the evaluated total capture cross section will be much larger than that in the current evaluated data files. Although the resonant components of the present evaluation are 2 to 3 times smaller than those in ENDF/B-VI, the total capture is much larger, at least in the energy ranges above 250 keV.

Table 10. The calculated average neutron capture cross sections of natural silicon

Energy range (keV)	Direct (mb)	Resonant (mb)		Total (mb)
		Present	ENDF/B-VI	
1–250	0.31	0.978	2.172	1.29 ± 0.18
250–450	0.50	0.212	0.532	0.71 ± 0.29
450–700	0.64	0.326	0.875	0.96 ± 0.37
700–1100	0.79	0.249	0.663	1.04 ± 0.47
1100–1450	0.95	0.142	0.336	1.09 ± 0.55
1450–1750	1.07	0.118	0.432	1.18 ± 0.62

VI. THE MAXWELLIAN AVERAGE CAPTURE CROSS SECTIONS

The Maxwellian average capture cross sections are input parameters to the stellar models. Several processes, the so-called *s*, *r*, and *p* processes, are used in the models to predict the abundances of the element in our solar system. New *s* process stellar models[20,21,22] indicate that most of the neutron exposure occurs at much lower temperature (kT = 6-8 keV) than previously thought (kT = 30 keV). Most previous neutron capture measurements, and many new high-precision measurements, did not extend to low enough energies to determine the reaction rate at these low temperatures; hence extrapolated rates were used. As far as the silicon isotopes are concerned, the new ORELA data indicate that extrapolations are in error by 2 or 3 times the estimated uncertainties.

The Maxwellian averaged cross sections of the silicon isotopes calculated from the present evaluation are compiled in Table 11 for kT ranging from 2 to 1180 keV. The cross sections consist of two parts:

firstly, the contribution from the resonance parameters, and secondly, the direct capture component. Since the direct capture calculation has a very large uncertainty compared with the experimental capture data, the errors on the average Maxwellian cross sections are dominated by the uncertainty of the direct capture calculation. The impact of the new Maxwellian average capture cross sections on the origin of presolar mainstream SiC was investigated, and the results are given in Ref. 23.

Table 11. The Maxwellian averaged capture cross sections

kT (keV)	^{28}Si (mb)	^{29}Si (mb)	^{30}Si (mb)
2	0.579 ± 0.108	1.209 ± 0.261	20.732 ± 2.04
5	0.410 ± 0.091	8.287 ± 0.842	14.997 ± 1.47
8	0.442 ± 0.090	11.219 ± 1.131	9.146 ± 0.900
10	0.530 ± 0.092	11.766 ± 1.191	6.941 ± 0.688
12	0.653 ± 0.095	11.787 ± 1.201	5.469 ± 0.552
15	0.859 ± 0.102	11.299 ± 1.170	4.052 ± 0.431
17.5	1.016 ± 0.107	10.672 ± 1.126	3.295 ± 0.375
20	1.148 ± 0.113	9.984 ± 1.079	2.769 ± 0.344
23	1.268 ± 0.118	9.173 ± 1.029	2.338 ± 0.327
25	1.328 ± 0.122	8.666 ± 1.001	2.134 ± 0.323
30	1.423 ± 0.129	7.560 ± 0.952	1.816 ± 0.326
35	1.465 ± 0.135	6.679 ± 0.930	1.669 ± 0.338
40	1.474 ± 0.140	5.988 ± 0.927	1.614 ± 0.354
45	1.465 ± 0.145	5.445 ± 0.937	1.608 ± 0.371
50	1.445 ± 0.149	5.016 ± 0.956	1.626 ± 0.387
52	1.436 ± 0.151	4.870 ± 0.965	1.637 ± 0.394
60	1.391 ± 0.157	4.398 ± 1.006	1.683 ± 0.419
70	1.332 ± 0.165	3.995 ± 1.064	1.733 ± 0.449
85	1.249 ± 0.176	3.624 ± 1.154	1.775 ± 0.489
100	1.179 ± 0.187	3.417 ± 1.242	1.785 ± 0.526
104	1.162 ± 0.190	3.379 ± 1.265	1.784 ± 0.535
149	1.029 ± 0.220	3.212 ± 1.502	1.737 ± 0.631
150	1.027 ± 0.221	3.212 ± 1.507	1.736 ± 0.633
180	0.975 ± 0.240	3.225 ± 1.647	1.705 ± 0.690

VII. BENCHMARK CALCULATIONS

To test the effect of the present evaluation in reactor calculations, in particular for criticality safety applications, some benchmark calculations were performed. Preliminary results are found in another

publication.[24] The benchmarks used are five critical configurations with heterogeneous combinations of highly enriched uranium, silicon dioxide, and polyethylene. The benchmark experiments were performed at the Institute for Physics and Power Engineering (IPPE),[25] Obninsk, Russia. They are intended to describe criticality safety of nuclear systems in which mixtures of uranium and silicon are present. The benchmark experiments are named BFS-79/1, BFS-79/2, BFS-79/3, BFS-79/4, and BFS-79/5. The neutron spectra for the BFS-79/1, BFS-79/3, and BFS-79/5 benchmarks are shown in Fig. 24. The spectra for the BFS-79/1 and the BFS-79/3 have a strong component in the thermal region, whereas for the BFS-79/5 benchmark the neutron spectrum peaks in the intermediate- and high-energy regions. The k_{eff} values were calculated for the five critical experiments by using the MCNP code.[26] The cross section library used in the MCNP calculation is based on the ENDF/B-VI release 4 in which the silicon evaluation is based on the evaluation done by Hetrick *et al*. at ORNL. The new evaluation for silicon was obtained by replacing the resonance parameters of the existing silicon evaluation in the ENDF/B-VI.4 with the new resonance parameter evaluation done at ORNL. This new ENDF evaluation was processed with the NJOY code[27] to generate a library in the format suitable to the MCNP code and was added to the MCNP library. The results of k_{eff} calculations using the MCNP library and the new silicon evaluation are given in Table 12. Table 12 indicates a slight improvement in the k_{eff} for the BFS-79/1, BFS-79/2, and BFS-79/3 benchmarks.

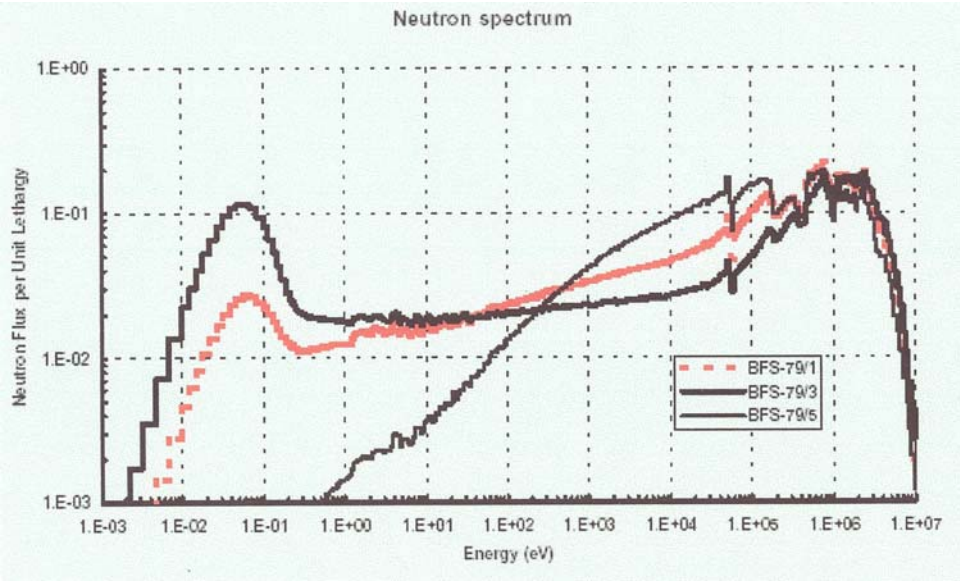

Fig. 24. Neutron flux spectra in the BFS-79 benchmark calculations.

Table 12. MCNP calculations of k_{eff} for the BFS benchmark systems

Experiment	Measured	MCNP ENDF/B-VI (MCNP, library release 4)	MCNP ENDF/B-VI (MCNP, library release 4, with silicon evaluation done at ORNL)
BFS-79/1	1.0007 ± 0.0027	1.0057 ± 0.0005	1.0038 ± 0.0005
BFS-79/2	1.0003 ± 0.0028	1.0153 ± 0.0005	1.0148 ± 0.0005
BFS-79/3	1.0012 ± 0.0029	1.0149 ± 0.0005	1.0139 ± 0.0005
BFS-79/4	1.0016 ± 0.0030	1.0073 ± 0.0005	1.0078 ± 0.0005
BFS-79/5	1.0005 ± 0.0040	1.0010 ± 0.0005	1.0027 ± 0.0005

In addition to the MCNP calculations we have also performed sensitivity calculations of the BFS benchmarks using the sensitivity analysis code SAMS[28] (Sensitivity Analysis Module for SCALE). SAMS combines problem-dependent cross sections generated in the SCALE system sequence, BONAMI, NITAWL, and KENO-V.a,[29] with forward and adjoint fluxes required to perform sensitivity calculations using linear perturbation theory. The calculations were done with the neutron 238-group structure of the SCALE system. The relative changes of k_{eff} for changes in the cross section as a function of the energy groups are given by the sensitivity coefficients, which are defined as

$$S_{g,x} = \frac{\left(\frac{dk}{k}\right)_{g,x}}{\left(\frac{d\sigma}{\sigma}\right)_{g,x}},$$

where g is the energy group and *x* is the type of cross section, namely, total, fission, capture, etc. The capture sensitivity coefficients for silicon and ^{235}U were calculated for BFS-79/1, BFS-79/2, and BFS-79/5 for the 238-group structure, and the results are shown in Fig. 25.

Figure 25 indicates that the BFS benchmarks are sensitive to the ^{235}U cross sections. To verify the impact of the ^{235}U cross section in calculating the BFS benchmarks, a more recent ORNL ^{235}U evaluation was used. The existing ^{235}U evaluation in the MCNP library was replaced by the new ^{235}U evaluation and the resulting MCNP calculations of the BFS benchmarks are shown in Table 13. Clearly, the use of the more recent ^{235}U cross section improves the benchmark results significantly. Further studies are underway to determine other isotopes that are important in the calculations of the BFS benchmarks.

In summary, the k_{eff} results for the BFS benchmark systems indicate that the new silicon evaluation is adequate for criticality safety calculations.

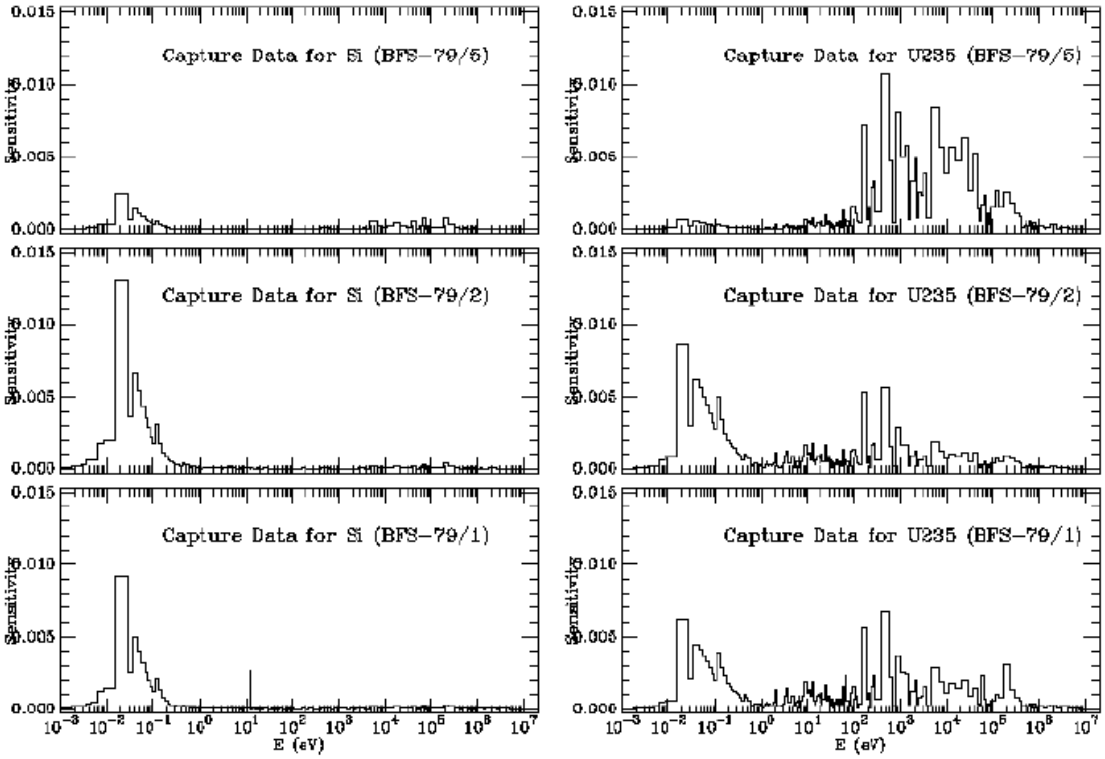

Fig. 25. Capture sensitivity coefficients calculated with the SAMS code for silicon and ^{235}U for the 238-group structure in the benchmark systems BFS-79/1, BFS-79/2, and BFS-79/5.

Table 13. MCNP calculations of k_{eff} for the BFS benchmark systems

Benchmark	Measured	MCNP ENDF/B-VI (MCNP, library release 4)	MCNP ENDF/B-VI (MCNP, library release 4, with silicon evaluation done at ORNL)	MCNP ENDF/B-VI (MCNP, library release 4, with silicon and ^{235}U evaluations done at ORNL)
BFS-79/1	1.0007 ± 0.0027	1.0057 ± 0.0005	1.0038 ± 0.0005	1.0021 ± 0.0005
BFS-79/2	1.0003 ± 0.0028	1.0153 ± 0.0005	1.0148 ± 0.0005	1.0131 ± 0.0005
BFS-79/3	1.0012 ± 0.0029	1.0149 ± 0.0005	1.0139 ± 0.0005	1.0122 ± 0.0005
BFS-79/4	1.0016 ± 0.0030	1.0073 ± 0.0005	1.0078 ± 0.0005	1.0060 ± 0.0005
BFS-79/5	1.0005 ± 0.0040	1.0010 ± 0.0005	1.0027 ± 0.0005	0.9990 ± 0.0005

VIII. CONCLUSION

The resonance parameters of the isotopes of silicon were reevaluated in the neutron energy range up to the neutron inelastic scattering threshold, using starting values from the ENDF/B-VI data (previous ORNL evaluation). Better accuracy was achieved by adding to the SAMMY experimental data base the results of the neutron capture measurements of natural silicon recently performed at ORELA in the energy range from 1 to 700 keV. Accurate values of the capture widths were obtained from the SAMMY analysis of the data in the energy range 1 to 700 keV, allowing the determination of reliable values of the average capture widths of the *s-, p-,* and *d*-waves resonances, at least for ^{28}Si, suitable for the normalization of the calculated resonant capture cross section in the resolved resonance region above 700 keV. Since the average capture cross sections of natural silicon between the resonances are small (less than 1 mb) and could not be measured with good accuracy due to the uncertainties in the experimental background and in other experimental effects, it was important to know the extent of the direct capture component compared with the average resonant component. Calculations were performed by T. Rauscher *et al*. in the energy range from thermal to about 1 MeV neutron energies and were available for the present evaluation. Actually, the direct average component is larger than the average resonant component in the energy ranges above 250 keV, and the resulting average total capture cross sections are significantly larger than those in ENDF/B-VI. In the present evaluation, the direct component was added to the file 3 of the ENDF/B-VI format.

Some problems remain to be investigated: (1) The thermal capture cross section of ^{28}Si relies mainly on the experimental value of Raman *et al*.[16] and on unpublished Kennett[18] results; the Islam value, which is about 25% larger, was disregarded in spite of its better performance in the benchmark calculations. (2) The direct capture component should be calculated with more accuracy due to its implication in the intermediate energy benchmark; the average value of the resonant capture component is much smaller than the direct component. (3) The ENDF/B-VI capture cross section of ^{29}Si in the unresolved energy region is very small compared with the direct capture component in the upper part of the resolved resonance region and should be reevaluated by using the TNG code in order to match the two regions.

REFERENCES

1. D. M. Hetrick *et al.*, *Evaluation of ^{28,29,30}Si Neutron Induced Cross Sections for ENDF/B-VI*, ORNL/TM-11825, Oak Ridge National Laboratory, Oak Ridge, Tenn., 1997.

2. N. M. Larson, *Updated Users' Guide for SAMMY: Multilevel R-Matrix Fits to Neutron Data Using Bayes' Equations*, ORNL/TM-9179/R4, Oak Ridge National Laboratory, Oak Ridge, Tenn., December 1998. See also ORNL/TM-9170/R5.

3. S. F. Mughabghab, M. Divadeenam, and N. E. Holden, *Neutron Cross Sections, Vol. 1, Neutron Resonance Parameters and Thermal Cross Sections, Part. A: Z = 1-60*, Academic Press, New York 1981.

4. K. H. Guber *et al.*, "Neutron Cross Section Measurements for Light Elements at ORELA and Their Application in Nuclear Criticality," Nuclear Data for Science and Technology, Tsukuda (Japan), Oct. 7-12, 2001, to be published as a supplement to the *Journal of Nuclear Science and Technology*.

5. J. A. Harvey, private communication (unpublished data taken in 1993).

6. D. C. Larson, C. H. Johnson, J. A. Harvey, and N. W. Hill, *Measurements of the Neutron Total Cross Section of Silicon from 5 eV 730 keV*, ORNL/TM-5618, Oak Ridge National Laboratory, Oak Ridge, Tenn., 1976.

7. F. G. Perey, T. A. Love, and W. E. Kinney, *A Test of Neutron Total Cross Section Evaluations from 0.2 to 20 MeV for C, O, Al, Si, Ca, Fe and SiO_2*, ORNL-4823, ENDF-178, Oak Ridge National Laboratory, Oak Ridge, Tenn., 1972.

8. J. A. Harvey *et al.*, *Phys. Rev. C* **28**, 24 (1983).

9. M. Adib *et al.*, *Atomkernenergie* **27**(2), 117 (1976).

10. N. M. Larson, L. C. Leal, and R. Q. Wright, "Proposal for Modification of ENDF Reich-Moore Format," CSEWG Meeting, November 3, 1999. See also the last update of ENDF-102, April 2001 (p. 2.46 and Appendix D).

11. R. O. Sayer *et al.*, *R-Matrix Evaluation of ^{16}O Neutron Cross Sections up to 6.3 MeV*, ORNL/TM-2000/212, Oak Ridge National Laboratory, Oak Ridge, Tenn., 2000.

12. P. E. Koehler *et al.*, *Phys. Rev. C* **62**, 055803 (2000).

13. J. W. Boldeman, B. J. Allen, A. R. Musgrove, and R. L. Macklin, *Nucl. Phys. A* **252**, 62 (1975).

14. T. Rauscher, private communication to K. H. Guber (1990).

15. H. Krauss, K. Grun, T. Rauscher, and H. Oberhummer, 1992, TU Wien (Vienna, Austria), code TEDCA, unpublished.

16. S. Raman, E. T. Jurney, J. W. Starner, and J. E. Lynn, *Phys. Rev. C* **46**, 972 (1992).

17. M. A. Islam, T. J. Kennett, and W. V. Prestwich, *Phys. Rev. C* **41**, 1272 (1990).

18. T. J. Kennett and W. V. Prestwich, private communication to S. Raman, 1992.

19. C. Y. Fu, *A Consistent Nuclear Model for Compound and Precompound Reactions with Conservation of Angular Momentum*, ORNL/TM-7042, Oak Ridge National Laboratory, Oak Ridge, Tenn., 1980.

20. F. Kappeler *et al.*, *Astrophys. J.*, **354**, 630 (1990).

21. G. Gallino, C. M. Gaiteri, and M. Busso, *Astrophys J.*, **410**, 400 (1993).

22. O. Straniero *et al.*, *Astrophys J.*, **440**, L85 (1995).

23. K. H. Guber *et al.*, "Maxwellian Average Neutron Capture Cross Sections for Silicon and their Impact on the Origin of Presolar Mainstream SiC Grains," submitted to *Physical Review C*.

24. T. E. Valentine, H. Derrien, L. C. Leal, and K. H. Guber, "Integration of Several Elements of the DOE Nuclear Criticality Safety Program," Nuclear Criticality Safety Topical Meeting 2001, Reno, Nevada, Nov. 11-15, 2001.

25. *International Handbook of Evaluated Criticality Safety Benchmark Experiments*, NEA/NDS/DOC (95) 03, Nuclear Energy Agency, OECD, Sept. 2000.

26. J. F. Briesmeister, Ed., *MCNP- A General Monte Carlo N-Particle Transport Code, Version 4C*, LA-13709-M, Los Alamos National Laboratory, Los Alamos, N.M., 2000.

27. R. E. MacFarlane, *The NJOY Nuclear Data Processing System Version 91,* LA-12740-M, Los Alamos National Laboratory, Los Alamos, N.M., October 1994. Available from the Radiation Safety Information Computational Center with the documentation for PSR-171/NJOY91.119.

28. B. T. Rearden, "SAMS: A Sensitivity Module for Criticality Safety Analysis Using Monte Carlo Techniques," *PHYSOR 2000*, May 7–12, 2000, Pittsburgh, Pennsylvania.

29. *SCALE: A Modular Code System for Performing Standardized Computer Analysis for Licencing and Evaluation*, NUREG/CR-0200, Rev.5 (ORNL/NUREG/CSD-2R5), Vols. I, II, and III, Oak Ridge National Laboratory, Oak Ridge, Tenn., March 1997. Available from the Radiation Safety Information Computational Center at ORNL as CCC-545.

INTERNAL DISTRIBUTION

1. Laboratory Records-RC, CRL, OSTI
2. Bryan L. Broadhead
3. Herve Derrien
4. Chia Y. Fu
5. Norman Maurice Greene
6. John A. Harvey
7. Joseph N. Herndon
8. Calvin M. Hopper
9. Ham T. Hunter
10. Daniel T. Ingersoll
11. Bernadette Lugue Kirk
12. Paul Edward Koehler
13. Nancy M. Larson
14. Luiz C. Leal
15. Cecil V. Parks
16. S. Ram Raman
17. Royce O. Sayer
18. Michael Scott Smith
19. Timothy E. Valentine
20. Robert Michael Westfall
21. RSICC

EXTERNAL DISTRIBUTION

22. H. Beer, Forschungszentrum Karlsruhe, IK, BAV 425, Postfach 3640, D-76021, Karlsruhe, Germany
23. P. Blaise, DER/SPRC/LEPH, Batiment 230, Centre d'Etudes de CADARACHE, 13108 Saint Paul-lez-Durance, France
24. R. Block, Rensselaer Polytechnic Institute, Troy, NY 12180-3590
25. O. Bouland, DER/SPRC/LEPH, Batiment 230, Centre d'Etudes de CADARACHE, 13108, Saint Paul-lez-Durance, France
26. D. Cabrilla, U.S. Department of Energy, NE-40, 19901 Germantown Road, Germantown, MD 20874-1290
27. D. E. Carlson, U.S. Nuclear Regulatory Commission, Reactor and Plant System Branch, Division of System Research, Office of Nuclear Regulatory Research, MS T-10 G6, RM T-10, 17, Washington, DC 20555-0001
28. C. Dunford, Brookhaven National Laboratory, Bldg 197D, National Nuclear Data Center, Upton, NY 11973
29. J. R. Felty, U.S. Department of Energy, DP-311, Washington , DC 20585
30. P. Finck, Argonne National Laboratory, Reactor Analysis Division, Bldg 208, Argonne, IL 60439
31. C. M. Frankle, Los Alamos National Laboratory, NIS-6MS J562, Los Alamos, NM 87545
32. F. Froehner, Kernforschungszentrum Karlsruhe, Inst f. Neutronenphysik und Reacktortechnik, Postfach 336 40, D-76021, Karlsruhe, Germany
33. W. Furman, Joint Inst. of Nuclear Research, P.O. Box 79, 141980 Dubna, Russian Federation
34. Srinivasan Ganesan, Head, Nuclear Data Section, Indira Gandhi Centre for Atomic Research, Kalpakkam 603 102, Tamilnadu, India
35. K. Guber, TÜV Energie und Systemtechnik GmbH Baden Würtemberg, Postfach 103262, D-68032 Mannheim, Germany
36. Frank Gunsing, Centre D'Etudes De Saclay, DSM/DAPNIA/SPhN, F-91191 Gif-sur-Yvette Cedex, France
37. G. M. Hale, Los Alamos National Laboratory, T-2, MS B243, Los Alamos, NM 87545
38. Akira Hasegawa, Nuclear Data Center, Japan Atomic Energy Research Institute, Tokai-mura, Naka-gun, lbaraki-ken 319-11, Japan
39. R. N. Hwang, Argonne National Laboratory, Reactor Analysis Division, Bldg 208., Argonne, IL 60439

40. R. P. Jacqmin, DER/SPRC/LEPH, Batiment 230, Centre d'Etudes de CADARACHE, 13408, Saint Paul-lez-Durance, France
41. N. Janeva, Bulgarian Academy of Sciences, 72, Boul, Tzarigradsko shosse, Sofia 1784, Bulgaria
42. F. Kappeler, Forschungszentrum Karlsruhe, IK, BAV 425, Postfach 3640, D-76021, Karlsruhe, Germany
43. R. Little, Los Alamos National Laboratory, X-TM, MS B226, Los Alamos, NM 87545
44. Lambros Lois, U.S. Nuclear Regulatory Commission, 08 E23, 11555 Rockville Pike, Rockville, MD 20852-2746
45. C. Lubitz, Knolls Atomic Power Laboratory, P. O. Box 1072, Schenectady, NY 12301
46. R. E. MacFarlane, Los Alamos National Laboratory, T-2, MS B243, Los Alamos, NM 87545
47. C. Mounier, CEN Saclay, DMT/SERMA/LENR, 91191 Gif Sur Yvette Cedex, France
48. C. Nordborg, OECDNEA, Le Seine St-Germain 12, Boulevard Iles, 92130, Issy-les-Moulineaux, France
49. C. Raepsaet, CEN Saclay, DST/DRECAM/LPS, 91191, Gif Sur Yvette Cedex, France
50. T. Rauscher, Institut fur Physik, Universitad Basel, Basel, Switzerland
51. E. Sartori, OECDNEA, Le Seine St-Germain 12, Boulevard Iles, 92130, Issy-les-Moulineaux, France
52. O. A. Shcherbakov, Petersburg Nuclear Physics Institute, 18 8 3 5 0 Gatchina, Leningrad District, Russia
53. R. Shelley, Central Bureau for Nuclear Measurements, Steenweg op Retie, 2240 Geel, Belgium
54. K. Shibata, Japan Atomic Energy Research Institute, Nuclear Data Center, Tokai-mura Naka-gun, Ibaraki-ken 319-11, Japan
55. A. B. Smith, Argonne National Laboratory, TD 362 D216, Argonne, IL 60544
56. H. Takano, Japan Atomic Energy Research Institute, Nuclear Data Center, Tokai-mura, Naka-gun, Ibaraki-ken 319-11, Japan
57. C. Wagemans, Central Bureau for Nuclear Measurements, Steenweg op Retie, 2240 Geel, Belgium
58. H. Weigmann, Central Bureau for Nuclear Measurements, Steenweg op Retie, 2240 Geel, Belgium
59. C. Werner, Rensselaer Polytechnic Institute, Residence Hall, 1999 Burdette Ave, Troy, NY 12180-3711
60. R. M. White, Lawrence Livermore National Laboratory, P. O. Box 808, Livermore, CA 94550
61. Phillip G. Young, Los Alamos National Laboratory, MS B243 T-16, Los Alamos, NM 87545